Chapter 6
The $g-2$ Experiments

6.1 Overview on the Principle of the Experiment

The main concepts and early results from the CERN muon storage ring experiment have been summarized in [1]. There are a number of excellent reviews on this subject and I am following in parts the ones of Combley, Farley and Picasso [2, 3] and of Vernon Hughes [4]. See also the more recent overviews [5, 6]. Many details on the experimental setup of the E821 experiment may be found in [7, 8], texts which were also very helpful. New experiments are on the way: one at Fermilab (E989) [9–11] in the US and another one at J-PARC (E34) [12–14] in Japan. While the Fermilab experiment represents a major upgrade of the Brookhaven experiment operating with **ultra relativistic muons** (as the later CERN experiments), the J-PARC experiment is planned to use **ultra cold muons** and will be the first precise experiment using a very different approach with rather different systematics.

The principle of the BNL muon $g-2$ experiment involves the study of the orbital and spin motion of highly polarized muons in a magnetic storage ring. This method has been applied in the last CERN experiment [15] already. The key improvements of the BNL experiment include the very high intensity of the primary proton beam from the proton storage ring AGS (Alternating Gradient Synchrotron), the injection of muons instead of pions into the storage ring, and a super–ferric storage ring magnet [16].

The muon $g-2$ experiment at Brookhaven works as illustrated in Fig. 6.1 [17–19]. Protons (mass about 1 GeV, energy 24 GeV) from the AGS hit a target and produce pions (of mass about 140 MeV). The pions are unstable and decay into muons plus a neutrino where the muons carry spin and thus a magnetic moment which is directed along the direction of the flight axis. The longitudinally polarized muons from pion decay are then injected into a uniform magnetic field **B** where they travel in a circle. The ring is a doughnut–shaped structure with a diameter of 14 m. A picture of the BNL muon storage ring is shown in Fig. 6.2. In the horizontal plane of the orbit the muons execute relativistic cyclotron motion with angular frequency ω_c. By the motion of the muon magnetic moment in the homogeneous magnetic field

F. Jegerlehner, *The Anomalous Magnetic Moment of the Muon*,
Springer Tracts in Modern Physics 274, DOI 10.1007/978-3-319-63577-4_6

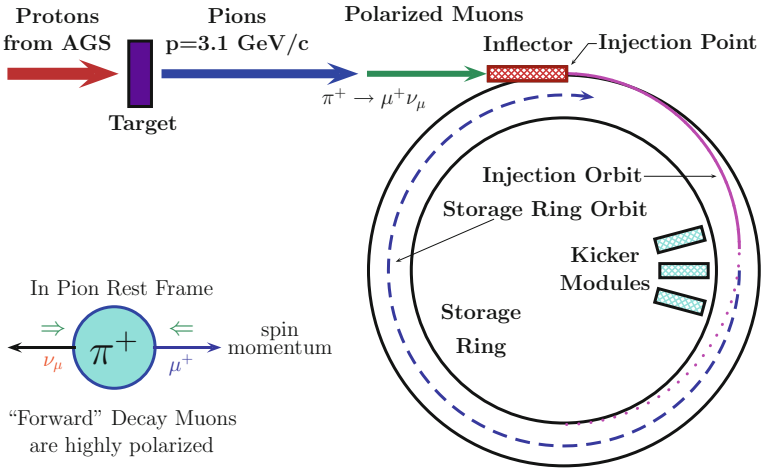

Fig. 6.1 The schematics of muon injection and storage in the $g-2$ ring

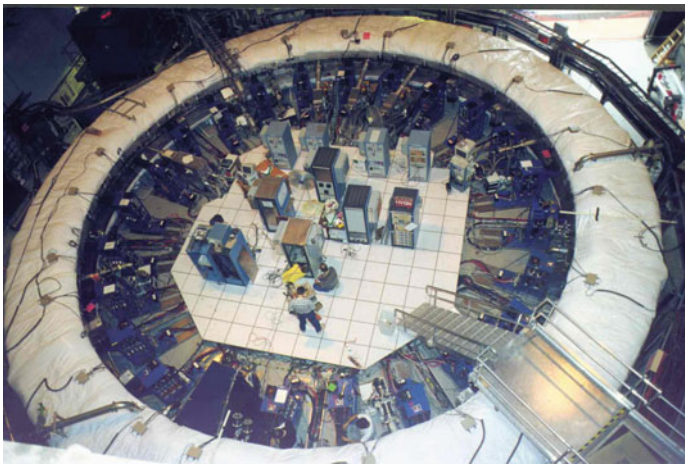

Fig. 6.2 The Brookhaven National Laboratory muon storage ring. The ring has a radius of 7.112 m, the aperture of the beam pipe is 90 mm, the field is 1.45 T and the momentum of the muon is $p_\mu = 3.094$ GeV/c. Picture taken from the Muon $g-2$ Collaboration Web Page http://www.g-2.bnl.gov/ (Courtesy of Brookhaven National Laboratory)

the spin axis is changed in a particular way as described by the Larmor precession. After each circle the muon's spin axis changes by 12' (arc seconds), while the muon is traveling at the same momentum (see Fig. 3.1). The muon spin is precessing with angular frequency ω_s, which is slightly bigger than ω_c by the difference angular frequency $\omega_a = \omega_s - \omega_c$.

$$\omega_c = \frac{eB}{m_\mu c\,\gamma}\,,$$
$$\omega_s = \frac{eB}{m_\mu c\,\gamma} + \frac{e}{m_\mu c}\,a_\mu\,B\,,$$
$$\omega_a = \frac{e}{m_\mu c}\,a_\mu\,B\,, \tag{6.1}$$

where $a_\mu = (g_\mu - 2)/2$ is the muon anomaly and $\gamma = 1/\sqrt{1 - v^2/c^2}$ is the relativistic Lorentz factor, v the muon velocity.[1] In the experiment ω_a and B are measured. The muon mass m_μ is obtained from an independent experiment on muonium, which is a $(\mu^+ e^-)$ bound system. Note that if the muon would just have its Dirac magnetic moment $g = 2$ (tree level) the direction of the spin of the muon would not change at all.

In order to retain the muons in the ring an electrostatic focusing system is needed. In reality in addition to the magnetic field **B** an electric quadrupole field **E** in the plane normal to the particle orbit is applied, which changes the angular frequency according to the Thomas-Bargmann–Michel–Telegdi (BMT) equation

$$\boldsymbol{\omega_a} = \frac{e}{m_\mu c}\left(a_\mu \mathbf{B} - \left[a_\mu - \frac{1}{\gamma^2 - 1}\right]\frac{\mathbf{v}\times\mathbf{E}}{c^2}\right)\,. \tag{6.2}$$

Interestingly, one has the possibility to choose γ such that $a_\mu - 1/(\gamma^2 - 1) = 0$, in which case ω_a becomes independent of **E**. This is the so–called *magic* γ. The muons are rather unstable and decay spontaneously after some time. When running at the magic energy the muons are highly relativistic, they travel almost at the speed of light with energies of about $E_{\text{magic}} = \gamma m_\mu c^2 \simeq 3.098\,\text{GeV}$. This rather high energy is dictated by the need of a large time dilatation on one hand and by the requirement to minimize the precession frequency shift caused by the electric quadrupole superimposed upon the uniform magnetic field. The magic γ-factor is about $\gamma = \sqrt{1 + 1/a_\mu} = 29.3$; the lifetime of a muon at rest is 2.19711 μs (micro seconds), while in the ring it is 64.435 µs (theory) [64.378 µs (experiment)]). Thus, with their lifetime being much larger than at rest, muons are circling in the ring many times before they decay into a positron plus two neutrinos: $\mu^+ \to e^+ + \nu_e + \bar{\nu_\mu}$. Since parity is violated maximally in this weak decay there is a strong correlation between the muon spin direction and the direction of emission of the positrons. The differential decay rate for the muon in the rest frame is given by (see also (2.47) and (6.57) below)

$$\mathrm{d}\Gamma^\pm/\Gamma = N(E_e)\left(1 \pm \frac{2x-1}{3-2x}\,\cos\theta\right)\mathrm{d}x\,\mathrm{d}\cos\theta\,, \tag{6.3}$$

in which E_e is the positron energy, x is E_e in units of the maximum energy $m_\mu/2$, Γ the total decay width (4.38), $N(E_e)$ is a normalization factor

[1] Formulas like (6.1) presented in this first overview will be derived below.

$$N(E_e) = 2x^2(3-2x) \ ,$$

and θ the angle between the positron momentum in the muon rest frame and the muon spin direction. At tree level $\Gamma = \tau_\mu^{-1} = G_\mu^2 m_\mu^5/192\pi^3$. The μ^+ decay spectrum is peaked strongly for small θ due to the non–vanishing coefficient of $\cos\theta$

$$A(E_e) = \frac{2x-1}{3-2x} \ ,$$

which is called asymmetry factor and reflects the *parity violation*.

The positron is emitted along the spin axis of the muon as illustrated in Fig. 6.3. The decay positrons are detected by 24 lead/scintillating fiber calorimeters spread evenly around inside the muon storage ring. These counters measure the positron energy and provide the direction of the muon spin. The number of decay positrons with energy greater than E_{th} emitted at time t after muons are injected into the storage ring is

$$N(t) = N_0(E_{\text{th}}) \ \exp\left(\frac{-t}{\gamma\tau_\mu}\right) \ [1 + A(E_{\text{th}}) \ \sin(\omega_a t + \phi(E_{\text{th}}))] \ , \tag{6.4}$$

where $N_0(E_{\text{th}})$ is a normalization factor, τ_μ the muon life time (in the muon rest frame), and $A(E_{\text{th}})$ is the asymmetry factor for positrons of energy $E > E_{\text{th}}$. A typical example for the time structure from the BNL experiment is shown in Fig. 6.4. As we see the exponential decay law for the decaying muons is modulated by the $g-2$ angular frequency. In this way the angular frequency ω_a is neatly determined

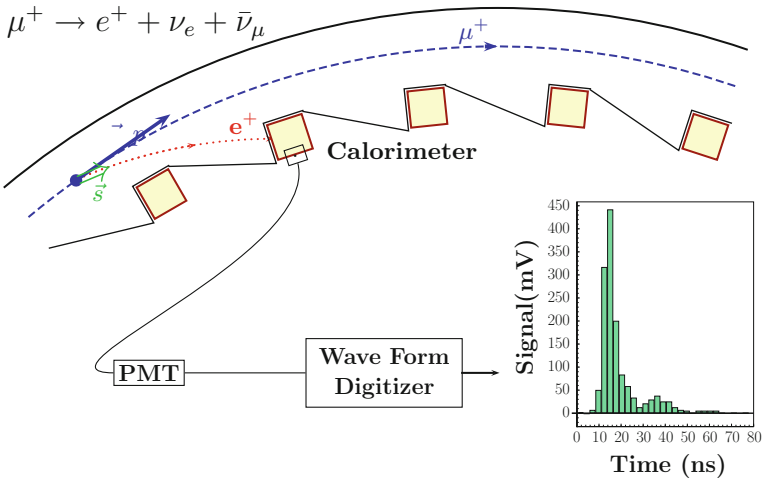

Fig. 6.3 Decay of μ^+ and detection of the emitted e^+ (PMT = Photomultiplier)

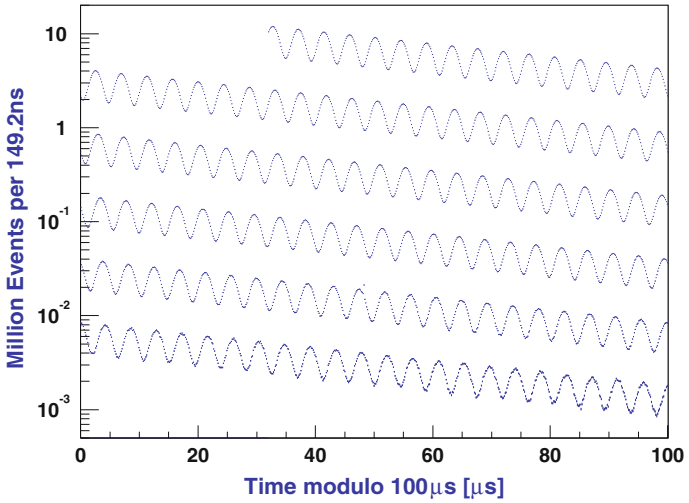

Fig. 6.4 Distribution of counts versus time for the 3.6 billion decays in the 2001 negative muon data–taking period Courtesy of the E821 collaboration. Reprinted with permission from [16]. Copyright (2007) by the American Physical Society

from the time distribution of the decay positrons observed with the electromagnetic calorimeters [20–24].

The magnetic field is measured by *Nuclear Magnetic Resonance* (NMR) using a standard probe of H_2O [25]. This standard can be related to the magnetic moment of a free proton by

$$B = \frac{\hbar\omega_p}{2\mu_p} \,, \tag{6.5}$$

where ω_p is the Larmor spin precession angular velocity of a proton in water. Using this, the frequency ω_a from (6.4), (6.1) and $\mu_\mu = (1 + a_\mu)\, e\hbar/(2m_\mu c)$, one obtains

$$a_\mu = \frac{R}{\lambda - R} \,, \tag{6.6}$$

where

$$R = \omega_a/\omega_p \quad \text{and} \quad \lambda = \mu_\mu/\mu_p \,. \tag{6.7}$$

The BNL experiment E-821 has determined

$$\bar{R} = \omega_a/\tilde{\omega}_p = 0.003\,707\,206\,4(20) \,, \tag{6.8}$$

where $\bar{R}$, assuming CPT invariance, is the weighted average of the results obtained separately for positive and negative muons, and $\tilde{\omega}_p$ is the proton cyclotron frequency in the average magnetic field along the storage ring. The quantity λ appears because

the value of the muon mass m_μ is needed, and also because the B field measurement involves the proton mass m_p. Measurements of the microwave spectrum of ground state muonium (μ^+e^-) [26] at LAMPF at Los Alamos, in combination with the theoretical prediction of the Muonium hyperfine splitting $\Delta\nu$ [27–29] (and references therein), have provided the precise (new CODATA 2011 recommended) value [30]

$$\frac{\mu_\mu}{\mu_p} = \lambda = 3.183\,345\,107(84)\ (30\,\text{ppb})\ , \tag{6.9}$$

which is to be used together with the E821 measurement of R to determine a_μ via (6.6). More details on the hyperfine structure of muonium will be given below in Sect. 6.6.

Since the spin precession frequency can be measured very well, the precision at which $g-2$ can be measured is essentially determined by the possibility to manufacture a constant homogeneous magnetic field **B** and to determine its value very precisely. An example of a field map from the BNL experiment is shown in Fig. 6.5. Important but easier to achieve is the tuning to the magic energy. Possible deviations may be corrected by adjusting the effective magnetic field appropriately.

In the following we will discuss various aspects mentioned in this brief overview in more detail: beam dynamics, spin precession dynamics, some theory background about the properties of the muon. This should shed some more light on the muon spin physics as it derives from the SM. A summary of the main experimental results and two short addenda on the ground state hyperfine structure of muonium and on single electron dynamics and the electron $g-2$ will close this part on the experimental principles.

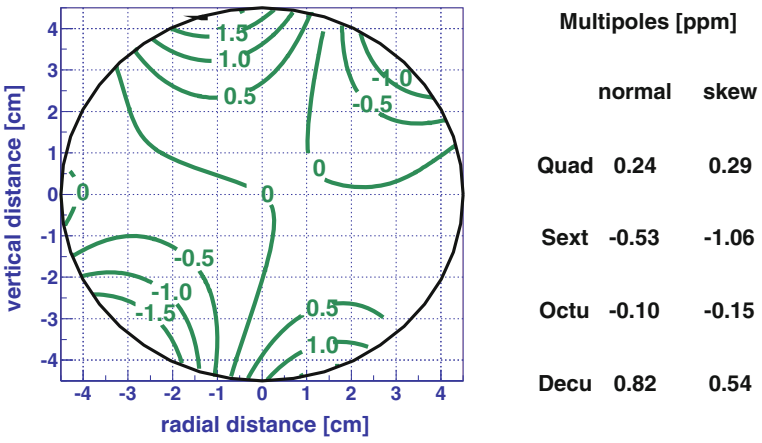

Fig. 6.5 Magnetic field profile. The contours are averaged over azimuth and interpolated using a multi–pole expansion. The circle indicates the storage aperture. The *contour lines* are separated by 1 ppm deviations from the central average Courtesy of the E821 collaboration [16]

6.2 Particle Dynamics

The anomalous magnetic moment of both electrons and muons are measured by observing the motion of charged particles in a type of Penning trap, which consists of an electrical quadrupole field superimposed upon a uniform magnetic field. The configurations used in these experiments have axial symmetry. The orbital motion of charged particles in the storage ring may be discussed separately from the spin motion because the forces associated with the anomalous magnetic moment are very weak ($a_\mu \approx 1.16 \times 10^{-3}$) in comparison to the forces of the charge of the particle determining the orbital motion. The force $\mathbf{F}$ on a particle of charge e of velocity $\mathbf{v}$ in fields $\mathbf{E}$ and $\mathbf{B}$ is given by the Lorentz force

$$\mathbf{F} = \frac{\mathrm{d}\mathbf{p}}{\mathrm{d}t} = e\ (\mathbf{E} + \mathbf{v} \times \mathbf{B})\ . \tag{6.10}$$

In a uniform magnetic field $\mathbf{B}$ of magnitude B_0 the particle with relativistic energy E_0 moves on a circle of radius

$$r_0 = \frac{E_0}{ecB_0}\ , \quad E_0 = \gamma mc^2\ . \tag{6.11}$$

Since we are interested in the dynamics of the muon beam in a ring, we consider a cylindrically symmetric situation. The cylindrical coordinates: $r = \sqrt{x^2 + y^2}$, θ, z are the radial, azimuthal and vertical coordinates of the particle position as shown in Fig. 6.6.

The relativistic equation of motion for the muon in the static cylindrical fields $\mathbf{B}(r, z)$ and $\mathbf{E}(r, z)$ takes the form

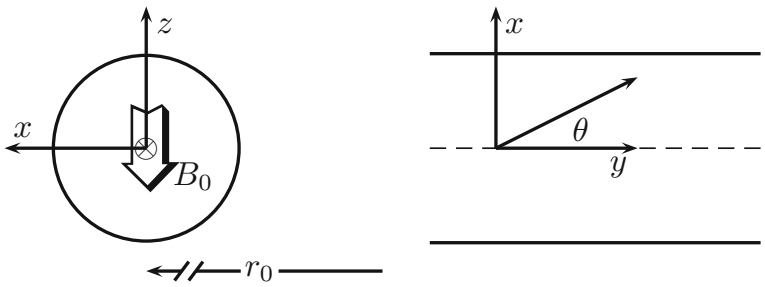

Fig. 6.6 Coordinates for the beam dynamics. View at the beam end (*left*) $x = r - r_0$ radial, z vertical, with B field in $-z$ direction; $(x, z) = (0, 0)$ is the beam position, the negative muon beam points into the plane. View from top (*right*) y is the direction along the beam

$$\frac{\mathrm{d}}{\mathrm{d}t}(m\dot{r}) = mr\dot{\theta}^2 - er\dot{\theta}B_z + eE_r \,, \tag{6.12}$$

$$\frac{\mathrm{d}}{\mathrm{d}t}(mr^2\dot{\theta}) = 0 \,, \tag{6.13}$$

$$\frac{\mathrm{d}}{\mathrm{d}t}(m\dot{z}) = er\dot{\theta}B_r + eE_z \,. \tag{6.14}$$

The general form of the electrostatic potential applied is

$$V(r,z) = \frac{V_0}{d^2}\left[r^2 - 2r_0^2 \ln\frac{r}{r_0} - r_0^2 - 2z^2\right],$$

where r_0 is the radius of the circle on which $\partial V/\partial r = 0$. This potential is singular along the symmetry axis except in the case $r_0 = 0$. In the latter case

$$V(r,z) = \frac{V_0}{d^2}\left(r^2 - 2z^2\right) \,, \tag{6.15}$$

which is the potential used in an electron trap. Here $(r_0, 0)$ and $(0, z_0)$ are the coordinates of the plates and $d^2 = r_0^2 + 2z_0^2$ (for a symmetric trap $r_0 = \sqrt{2}z_0$).

In the muon $g-2$ experiment $r \to x = r - r_0$ with $|x| \ll r_0$ (see Fig. 6.6) and weak focusing is implemented by a configuration of charged plates as shown in Fig. 6.7. In order to get a pure quadrupole field one has to use hyperbolic plates with end–caps $z^2 = z_0^2 + x^2/2$ and $z^2 = \frac{1}{2}(x^2 - x_0^2)$ on the ring. While the CERN experiment was using hyperbolic plates, the BNL one uses flat plates which produce 12– and 20–pole harmonics. The length of the electrodes is adjusted to suppress the 12–pole mode leaving a 2% 20–pole admixture. The electric field produces a restoring force in the vertical direction and a repulsive force in the radial direction:

$$\mathbf{E} = (E_r, E_\theta, E_z) = (\kappa x, 0, -\kappa z) \,, \tag{6.16}$$

where $x = r - r_0$ and κ a positive constant. In order to keep the beam focused, the restoring force of the vertical magnetic field must be stronger than the repulsive force

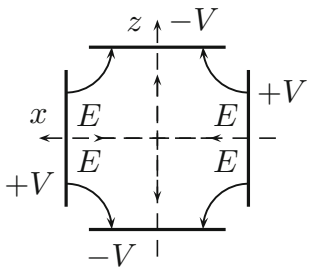

Fig. 6.7 Electric quadrupole field E. The vertical direction is z, the radial x ($x_0 = \sqrt{2}z_0$); $V = V_0/2$ at the plates

of the electrical field in the radial direction:

$$0 < \frac{eV_0}{d^2} < \frac{e^2B^2}{8mc} \,. \tag{6.17}$$

The radial force is

$$F_r = \frac{\gamma m v^2}{r} - \frac{e}{c} v B_z + eE_r \,, \tag{6.18}$$

and since on the equilibrium orbit $r = r_0$ and $E_r = 0$ we have

$$\frac{\gamma m v^2}{r_0} = \frac{e}{c} v B_z \,. \tag{6.19}$$

As r_0 is large relative to the beam spread, we may expand r about r_0:

$$\frac{1}{r} = \frac{1}{r_0 + x} \simeq \frac{1}{r_0}\left(1 - \frac{x}{r_0}\right) \,.$$

Therefore, using (6.19) we may write

$$F_x = F_r = -e\beta B_z\,(1-n)\,\frac{x}{r_0} \;\Rightarrow\; \gamma m\ddot{x} = -(1-n)\,\frac{\gamma m v^2}{r_0^2}\,x \,, \tag{6.20}$$

where $\beta = v/c$ and n is the field index

$$n = \frac{\kappa r_0}{\beta B_0} \,, \quad B_0 = B_z \,. \tag{6.21}$$

For the vertical motion we have

$$F_z = -e\kappa z \;\Rightarrow\; \gamma m\ddot{z} = -e\kappa z \,, \tag{6.22}$$

and with $\omega_0 = v/r_0$, using (6.19) and (6.21), the equations of motion take the form

$$\begin{aligned} &\ddot{x} + (1-n)\,\omega_0^2\,x = 0 \,, \\ &\ddot{z} + e\kappa\, z = 0 \,, \end{aligned} \tag{6.23}$$

with the oscillatory solutions

$$\begin{aligned} x &= A\,\cos(\sqrt{1-n}\,\omega_0\,t) \,, \\ z &= B\,\cos(\sqrt{n}\,\omega_0\,t) \,. \end{aligned} \tag{6.24}$$

We have used $e\kappa = n\omega_0^2$ following from (6.21). The amplitudes depend on the *initial condition* of the particle trajectory. This motion is called *betatron oscillation*. The betatron frequencies are $\omega_{y\mathrm{BO}} = \sqrt{n}\,\omega_c$ and $\omega_{x\mathrm{BO}} = \sqrt{1-n}\,\omega_c$ where $\omega_c = \omega_0 = v/r_0$ is the cyclotron frequency. In the experiment a lattice of quadrupoles is distributed along the ring. For the BNL experiment the lattice has a four–fold symmetry and the quadrupoles are covering 43% of the ring. The corresponding dynamics has to be calculated taking into account the geometry of the configuration, but follows the same principle.

The dynamics of an electron in a Penning trap and the principle of electron $g-2$ experiments will be considered briefly in Sect. 6.7 at the end of this part of the book.

6.3 Magnetic Precession for Moving Particles

The precession of spinning particles in magnetic fields is a classic subject investigated long time ago [31]. Our exposition follows closely Bell's lecture. In a magnetic field $\mathbf{B}$ the polarization $\mathbf{P}$ of a particle changes according to

$$\frac{\mathrm{d}\mathbf{P}}{\mathrm{d}t} = g\,\frac{e}{2m}\,\mathbf{P}\times\mathbf{B}\,,$$

the component of $\mathbf{P}$ parallel to $\mathbf{B}$ remains constant, while the part of $\mathbf{P}$ perpendicular to $\mathbf{B}$ rotates about $\mathbf{B}$ with angular frequency

$$\omega = g\,\frac{e}{2m}\,B\,, \tag{6.25}$$

the non–relativistic cyclotron frequency. This holds in the rest frame O of the particle. For moving and even fast–moving particles we may get the motion in the laboratory system O' by a Lorentz transformation. In a pure L–transformation $x^{\mu'} = L^{\mu}_{\ \nu}x^{\nu}$ $[x^{\mu} = (ct, \mathbf{x})]$ L has the form[2]

$$L = \begin{pmatrix} \gamma & -\gamma\frac{\mathbf{v}}{c} \\ -\gamma\frac{\mathbf{v}}{c} & \mathbf{1} + (\gamma-1)\,\mathbf{n}\,\mathbf{n}\cdot \end{pmatrix},$$

where $\mathbf{n} = \mathbf{v}/v$ and $\gamma = 1/\sqrt{1-v^2/c^2}$. For accelerated particles, the velocity is changing and in the next moment the velocity is $\mathbf{v}' = \mathbf{v} + \delta\mathbf{v}$. In the laboratory frame we thus have $x^{\mu'} = L^{\mu}_{\ \nu}(\mathbf{v})x^{\nu}$ and $x^{\mu''} = L^{\mu}_{\ \nu}(\mathbf{v}')x^{\nu}$ and expanding to linear order in $\delta\mathbf{v}$ one obtains the motion as seen in the laboratory frame as

$$\begin{aligned} t'' &= t' - \delta\mathbf{u}'\cdot\mathbf{x}'\,, \\ \mathbf{x}'' &= \mathbf{x}' + \delta\boldsymbol{\theta}'\times\mathbf{x}' - \mathbf{u}'t'\,, \end{aligned} \tag{6.26}$$

[2] L is a matrix operator acting on four–vectors. The $\cdot$ operation at the right of the spacial submatrix means forming a scalar product with the spatial part of the vector on which L acts.

with

$$\mathbf{u}' = \gamma \left(1 + \frac{\gamma - 1}{v^2}\, \mathbf{v}\, \mathbf{v}\cdot\right) \delta\mathbf{v}\,,$$
$$\delta\boldsymbol{\theta}' = \frac{\gamma - 1}{v^2}\, (\delta\mathbf{v} \times \mathbf{v})\ , \tag{6.27}$$

which tells us that from the two pure boosts we got an infinitesimal transformation which includes both a boost (pure if $\delta\boldsymbol{\theta}' = 0$) and a rotation (pure if $\mathbf{u}' = 0$). The transformation (6.26) is the infinitesimal law for transforming vectors in O' to vectors in O''.

The precession equation for accelerated moving particles is then obtained as follows: Let O' be the observer for whom the particle is momentarily at rest. If the particle has no electric dipole moment, what we assume (see end of Sect. 3.3), an electric field does not contribute to the precession and only serves to accelerate the particle

$$\delta\mathbf{u}' = \frac{e}{m}\, \mathbf{E}'\, \delta t'\ , \tag{6.28}$$

while the magnetic field provides the precession

$$\delta\mathbf{P}' = -g\frac{e}{2m}\, \mathbf{B}' \times \mathbf{P}'\, \delta t'\ . \tag{6.29}$$

In the laboratory frame O' the observed polarization is $\mathbf{P}' + \delta\mathbf{P}'$ where $\mathbf{P}' = \mathbf{P}$ is the polarization of the particle in its rest frame O. The observer O'' by a boost from O sees a polarization $\mathbf{P}'' + \delta\mathbf{P}''$ which differs by a rotation $\delta\boldsymbol{\theta}'$ from the previous one: (note that momentarily $\mathbf{P}'' = \mathbf{P}' = \mathbf{P}$)

$$\delta\mathbf{P}'' = \delta\mathbf{P}' + \delta\boldsymbol{\theta}' \times \mathbf{P}\,, \tag{6.30}$$

or

$$\delta\mathbf{P}'' = -g\frac{e}{2m}\, \mathbf{B}' \times \mathbf{P}\, \delta t' + \frac{(\gamma - 1)}{v^2}\, (\delta\mathbf{v} \times \mathbf{v}) \times \mathbf{P}\,. \tag{6.31}$$

The precession equation in the laboratory frame may be obtained by applying the L–transformations of coordinates and fields to the lab frame:

$$\delta t' = \gamma \left(\delta t - \frac{\mathbf{v}\cdot\delta\mathbf{x}}{c^2}\right) = \gamma\, \delta t \left(1 - \frac{v^2}{c^2}\right) = \frac{1}{\gamma}\delta t\,,$$
$$\mathbf{B}' = \gamma \left(\mathbf{B} - \frac{\mathbf{v}\times\mathbf{E}}{c^2}\right) + \frac{(1-\gamma)}{v^2}\, \mathbf{v}\cdot\mathbf{B}\, \mathbf{v}\,,$$
$$\mathbf{E}' = \gamma\, (\mathbf{E} + \mathbf{v}\times\mathbf{B}) + \frac{(1-\gamma)}{v^2}\, \mathbf{v}\cdot\mathbf{E}\, \mathbf{v}\,, \tag{6.32}$$

and one obtains

$$\frac{\mathrm{d}\mathbf{P}}{\mathrm{d}t} = \boldsymbol{\omega}_s \times \mathbf{P}\,, \tag{6.33}$$

with

$$\boldsymbol{\omega}_s = \frac{\gamma-1}{v^2}\frac{\mathrm{d}\mathbf{v}}{\mathrm{d}t}\times\mathbf{v} - g\frac{e}{2m}\left(\mathbf{B} - \frac{\mathbf{v}\times\mathbf{E}}{c^2} + \frac{1-\gamma}{\gamma v^2}\,\mathbf{v}\cdot\mathbf{B}\,\mathbf{v}\right)\,. \tag{6.34}$$

The first term, which explicitly depends on the acceleration, is called *Thomas precession*. The acceleration in the laboratory frame may be obtained in the same way from (6.28) together with (6.27) and (6.32)

$$\frac{\mathrm{d}\mathbf{v}}{\mathrm{d}t} = \frac{e}{\gamma m}\,(\mathbf{E}+\mathbf{v}\times\mathbf{B}) - \frac{e}{\gamma m c^2}\,\mathbf{v}\cdot\mathbf{E}\,\mathbf{v}\,, \tag{6.35}$$

which is just another form of the usual equation of motion[3] (Lorentz force)

$$\frac{\mathrm{d}\mathbf{p}}{\mathrm{d}t} = \frac{\mathrm{d}}{\mathrm{d}t}\,(\gamma m\mathbf{v}) = e\,(\mathbf{E}+\mathbf{v}\times\mathbf{B})\,.$$

If one uses (6.35) to eliminate the explicit acceleration term from (6.34) together with $(\mathbf{v}\times\mathbf{B})\times\mathbf{v} = \mathbf{B}v^2 - \mathbf{v}\cdot\mathbf{B}\mathbf{v}$ and $\mathbf{v}\times\mathbf{v} = 0$, one obtains

$$\boldsymbol{\omega}_s = -\frac{e}{\gamma m}\left\{(1+\gamma a)\,\mathbf{B} + \frac{(1-\gamma)}{v^2}\,a\,\mathbf{v}\cdot\mathbf{B}\,\mathbf{v} + \gamma\left(a+\frac{1}{\gamma+1}\right)\frac{\mathbf{E}\times\mathbf{v}}{c^2}\right\}\,, \tag{6.36}$$

where $a = g/2-1$ is the anomaly term.

6.3.1 $g-2$ Experiment and Magic Momentum

In the $g-2$ experiment one works with purely transversal fields: $\mathbf{v}\cdot\mathbf{E} = \mathbf{v}\cdot\mathbf{B} = 0$. Then using $(\mathbf{v}\times\mathbf{E})\times\mathbf{v} = v^2\,\mathbf{E}$ (when $\mathbf{v}\cdot\mathbf{E}=0$) and $v^2/c^2 = (\gamma^2-1)/\gamma^2$ the equation of motion can be written

$$\frac{\mathrm{d}\mathbf{v}}{\mathrm{d}t} = \boldsymbol{\omega}_c\times\mathbf{v}\,,\quad \boldsymbol{\omega}_c = -\frac{e}{\gamma m}\left(\mathbf{B} + \frac{\gamma^2}{\gamma^2-1}\,\frac{\mathbf{E}\times\mathbf{v}}{c^2}\right)\,. \tag{6.37}$$

[3] Note that $\mathrm{d}\,\gamma = \gamma^3\,\mathbf{v}\cdot\mathrm{d}\mathbf{v}/c^2$ and the equation of motion implies

$$\mathbf{v}\cdot\frac{\mathrm{d}\,(\gamma m\mathbf{v})}{\mathrm{d}t} = m\gamma^3\mathbf{v}\cdot\frac{\mathrm{d}\mathbf{v}}{\mathrm{d}t} = e\,\mathbf{v}\cdot\mathbf{E}\,,$$

as $\mathbf{v}\cdot(\mathbf{v}\times\mathbf{B})\equiv 0$. This has been used in obtaining (6.35).

The velocity $\mathbf{v}$ thus rotates, without change of magnitude, with the relativistic cyclotron frequency $\boldsymbol{\omega}_c$. The precession of the polarization $\mathbf{P}$, which is to be identified with the muon spin $\mathbf{S}_\mu$, for purely transversal fields is then

$$\boldsymbol{\omega}_a = \boldsymbol{\omega}_s - \boldsymbol{\omega}_c = -\frac{e}{m}\left\{a\,\mathbf{B} + \left(a - \frac{1}{\gamma^2 - 1}\right)\frac{\mathbf{E}\times\mathbf{v}}{c^2}\right\}. \tag{6.38}$$

This establishes the key formula for measuring a_μ, which we have used and discussed earlier. It was found by Bargmann, Michel and Telegdi in 1959 [31] (see also [32] for a recent reconsideration). Actually, the magnetic transversality condition $\mathbf{v}\cdot\mathbf{B} = 0$ due to electrostatic focusing is not accurately satisfied (pitch correction) such that the more general formula

$$\boldsymbol{\omega}_a = -\frac{e}{m}\left\{a\,\mathbf{B} - a\left(\frac{\gamma}{\gamma+1}\right)\frac{\mathbf{v}\cdot\mathbf{B}\mathbf{v}}{c^2} + \left(a - \frac{1}{\gamma^2-1}\right)\frac{\mathbf{E}\times\mathbf{v}}{c^2}\right\}, \tag{6.39}$$

has to be used.

Since the anomalous magnetic moment for leptons is a very small quantity $a \approx 1.166 \times 10^{-3}$, electrons and muons in a pure magnetic field and initially polarized in the direction of motion ($\mathbf{P} \propto \mathbf{v}$) only very slowly develop a component of polarization transverse to the direction of motion. The observation of this development provides a sensitive measure of the small but theoretically very interesting anomalous magnetic moment.

In the original muon $g-2$ experiments only a $\mathbf{B}$ field was applied and in order to give some stability to the beam the $\mathbf{B}$ was not quite uniform,[4] and the particles oscillate about an equilibrium orbit. As a result one of the main limitations of the precision of those experiments was the difficulty to determine the effective average $\mathbf{B}$ to be used in calculating a_μ from the observed oscillation frequencies. To avoid this, in the latest CERN experiment, as later in the BNL experiment, the field $\mathbf{B}$ is chosen as uniform as possible and focusing is provided by transverse electric quadrupole fields. To minimize the effect of the electric fields on the precession of $\mathbf{P}$, muons with a special "magic" velocity are used so that the coefficient of the second term in (6.37) is small:

$$a_\mu - \frac{1}{\gamma^2 - 1} \approx 0\,,$$

corresponding to a muon energy of about 3.1 GeV. This elegant method for measuring a_μ was proposed by Bailey, Farley, Jöstlein, Picasso and Wickens and realized as the last CERN muon $g-2$ experiment and later adopted by the experiment at BNL. The motion of the muons is characterized by the frequencies listed in Table 6.1.

Two small, but important, corrections come from the effect of the electric focusing field $\mathbf{E}$ on the spin precession ω_a.

[4] Magnetic focusing using an inhomogeneous field $B_z = B_0\,(r_0/r)^n$, which by Maxwell's equation $\nabla\times\mathbf{B} = 0$ implies $B_r \simeq -n/r_0\,B_0\,z$ for $r \simeq r_0$, leads to identical betatron oscillation equations (6.23) as electrostatic focusing.

Table 6.1 Frequencies and time periods in the muon $g-2$ experiment E821. The field index used is $n = 0.137$. It is optimized to avoid unwanted resonances in the muon storage ring

Type	$\nu_i = \omega_i/2\pi$	Expression	Frequency (MHz)	Period
Anomalous precession	ν_a	$\frac{ea_\mu B}{2\pi m}$	0.23	4.37 μs
Cyclotron	ν_c	$\frac{v}{2\pi r_0}$	6.71	149 ns
Horizontal betatron	ν_x	$\sqrt{1-n}\,\nu_c$	6.23	160 ns
Vertical betatron	ν_z	$\sqrt{n}\,\nu_c$	2.48	402 ns

The first is the *Radial Electric Field Correction*, the change in ω_a when the momentum p deviates from the magic value $p \neq p_m$ and hence $p = \beta\gamma m = p_m + \Delta p$. In fact, the beam is not monoenergetic and the momentum tune has a small uncertainty of about $\pm 0.5\%$. This effect can be corrected by a change in the effective magnetic field [15] used in extracting a_μ. In cylindrical coordinates Fig. 6.6 using $(\mathbf{v}\times\mathbf{E})_z = -v_y E_x = -vE_r$, as $E_y = 0$, we find $aB_z + (a - 1/(\beta^2\gamma^2))\, v\, E_r/c^2$ or, with $B_0 = -B_z > 0$,

$$B_{0\,\mathrm{eff}} = B_0 \left[1 - \beta\frac{E_r}{B_0}\left(1 - \frac{1}{a_\mu\beta^2\gamma^2}\right)\right] \equiv C_E\, B_0\ . \tag{6.40}$$

This directly translates into

$$\frac{\Delta\omega_a}{\omega_a} = C_E \simeq -2\frac{\beta E_r}{B_0}\left(\frac{\Delta p}{p_m}\right)\ . \tag{6.41}$$

One may apply furthermore the relation $\Delta p/p_m = (1-n)\,(x_e/r_0)$, where x_e is the equilibrium position of the particle relative to the center of the aperture of the ring. For the BNL experiment typically

$$C_E \simeq 0.5\ \mathrm{ppm}\ . \tag{6.42}$$

The second effect is the *Vertical Pitch Correction* arising from vertical betatron oscillations [3, 33]. The focusing force due to $\mathbf{E}$ changes v_z at the betatron oscillation frequency $\omega_p = \omega_{z\mathrm{BO}}$[5] such that

$$\psi(t) = \psi_0\ \sin\omega_p t\ . \tag{6.43}$$

The muon will follow a spiral path with pitch angle ψ (see Fig. 6.8) given by

[5]The pitch frequency here should not to be confused with the proton precession frequency ω_p appearing in (6.7).

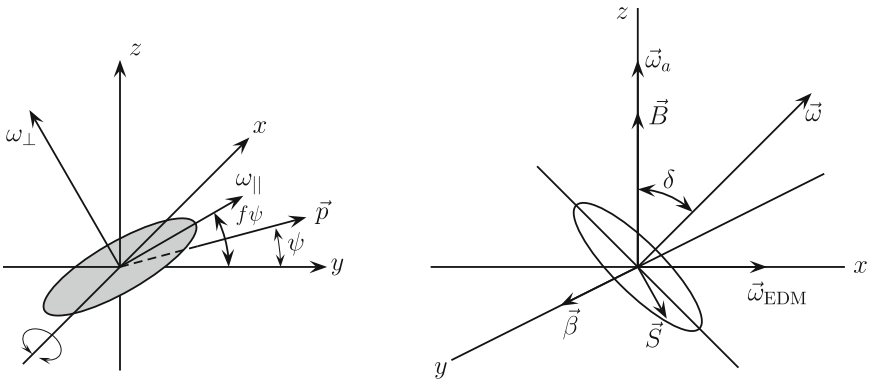

Fig. 6.8 *Left* frame for pitch correction. **p** lies always in the yz-plane. The pitch angle ψ between **p** and the y-axis (beam direction) oscillates. The spin **S** then rotates about the x-axis through an angle $f\psi$, where for electric focusing $f = 1 + \beta^2\gamma a - \gamma^{-1}$; $f = 1$ at magic γ. *Right* frame for EDM correction. As $|\mathbf{E}| \ll |\mathbf{E}^*| = c|\boldsymbol{\beta} \times \mathbf{B}|$, $\boldsymbol{\omega}_{\rm EDM}$ points along the x-axis while the unperturbed $\boldsymbol{\omega}_a$ points in z-direction. $\delta = \arctan \frac{\eta\beta}{2a} \simeq \frac{\eta}{2a}$

$$\frac{v_z}{v} = \sin\psi \simeq \psi\,, \tag{6.44}$$

and ω_a is changed. Now $\mathbf{v} \cdot \mathbf{B} \neq 0$, which persists as an effect from the focusing field also if running at the magic γ. The corresponding correction follows from (6.39), at $\gamma = \gamma_m$. The motion vertical to the main plane implies

$$\begin{aligned}\omega_{az} &= \frac{e}{m}\, a\, B_0 \left[1 - \left(\frac{\gamma}{\gamma+1}\right) \beta_z^2\right] \\ &= \omega_a \left[1 - \left(\frac{\gamma}{\gamma+1}\right) \beta^2 \frac{v_z^2}{v^2}\right] = \omega_a \left[1 - \left(\frac{\gamma-1}{\gamma}\right) \psi^2\right],\end{aligned} \tag{6.45}$$

where ω_a is the ideal (unperturbed) precession frequency. Similarly,

$$\begin{aligned}\omega_{ay} &= -\frac{e}{m}\, a\, B_0 \left[1 - \left(\frac{\gamma}{\gamma+1}\right) \beta_z\beta_y\right] \\ &= -\omega_a \left[1 - \left(\frac{\gamma}{\gamma+1}\right) \beta^2 \frac{v_z v_y}{v^2}\right] = -\omega_a \left[1 - \left(\frac{\gamma-1}{\gamma}\right) \psi\right],\end{aligned} \tag{6.46}$$

where we used

$$\frac{v_z}{v} = \sin\psi \simeq \psi\,, \quad \frac{v_y}{v} = \cos\psi \simeq 1\,.$$

The component of $\boldsymbol{\omega}_a$ parallel to the tilted plane changes sign and in the time average has no effect. The perpendicular component is

$$\omega_\perp = \omega_a = \omega_z \cos\psi - \omega_y \sin\psi \simeq \omega_z - \omega_y \psi\,, \tag{6.47}$$

and hence

$$\omega_a' = \omega_a\ (1 - C_P) = \omega_a \left(1 - \frac{\psi^2}{2}\right)\,. \tag{6.48}$$

In the time average by (6.43) $\overline{\psi}^2 = \frac{1}{2}\psi_0^2$ and thus $C_P = \frac{1}{4}\psi_0^2$. This holds provided $\omega_a \ll \omega_p$ otherwise the correction reads [33]

$$C_P = \frac{1}{4}\psi_0^2\,\beta^2 \left(1 - (a\beta\gamma)^2 \frac{\omega_p^2}{(\omega_a^2 - \omega_p^2)}\right)\,, \tag{6.49}$$

with $(a\beta\gamma)^2 = 1/(\beta\gamma)^2$ at magic γ. For the BNL experiment the pitch corrections is of the order

$$C_P \simeq 0.3\,\text{ppm}\,. \tag{6.50}$$

A third possible correction could be due to an EDM of the muon. If a large enough *electric dipole moment*[6]

$$\mathbf{d}_e = \frac{\eta\, e}{2mc}\mathbf{S}\,, \tag{6.51}$$

(see (1.5), p. 34 in Sect. 2.1.2 and the discussion at the end of Sect. 3.3) would exist the applied electric field $\mathbf{E}$ (which is vanishing at the equilibrium beam position) and the motional electric field induced in the muon rest frame $\mathbf{E}^* = \gamma\boldsymbol{\beta} \times \mathbf{B}$ would add an extra precession of the spin with a component along $\mathbf{E}$ and one about an axis perpendicular to $\mathbf{B}$:

$$\boldsymbol{\omega}_{a'} = \boldsymbol{\omega}_a + \boldsymbol{\omega}_{\text{EDM}} = \boldsymbol{\omega}_a - \frac{\eta\, e}{2m_\mu}\left(\frac{\mathbf{E}}{c} + \boldsymbol{\beta} \times \mathbf{B}\right)\,, \tag{6.52}$$

or

$$\Delta\boldsymbol{\omega}_a = -2d_\mu\ (\boldsymbol{\beta} \times \mathbf{B}) - 2d_\mu\,\mathbf{E}\,,$$

which, for $\beta \sim 1$ and $d_\mu\,\mathbf{E} \sim 0$, yields

$$\omega_{a'} = B\sqrt{\left(\frac{e}{m_\mu}\,a_\mu\right)^2 + \left(2d_\mu\right)^2}\,. \tag{6.53}$$

Note that η is the dimensionless constant equivalent of magnetic moment g-factors. The result is that the plane of precession in no longer horizontal but tilted at an angle

[6] Remembering the normalization: the magnetic and electric dipole moments are given by $\mu = \frac{g}{2}\,\frac{e\hbar}{2mc}$ and $d = \frac{\eta}{2}\,\frac{e\hbar}{2mc}$, respectively.

$$\delta \equiv \arctan \frac{\omega_{\rm EDM}}{\omega_a} = \arctan \frac{\eta\,\beta}{2a} \simeq \frac{\eta}{2a}\,, \tag{6.54}$$

and the precession frequency is increased by a factor

$$\omega_a' = \omega_a \sqrt{1+\delta^2}\,. \tag{6.55}$$

The tilt gives rise to an oscillating vertical component of the muon polarization, and may be detected by recording separately the electrons which strike the counters above and below the mid–plane of the ring. This measurement has been performed in the last CERN experiment on $g-2$, and has been repeated at BNL.

6.4 Theory: Production and Decay of Muons

For the $(g_\mu - 2)$ experiments one needs polarized muons. Basic symmetries of the weak interaction of the muons make it relatively easy to produce polarized muons. What helps is the maximal parity violation of the charged current weak interactions, mediated by the charged $W^\pm$ gauge bosons, which in its most pronounced form manifests itself in the "non–existence" of right–handed neutrinos ν_R. What it means more precisely is that right handed neutrinos are "sterile" in the sense that they do not interact with any kinds of the gauge bosons, which we know are responsible for electromagnetic (photon), weak (W- and Z-bosons) and strong (gluons) interactions of matter. It means that their production rate in ordinary weak reactions is practically zero which amounts to lepton number conservation for all practical purposes in laboratory experiments.[7]

Pion production may be done by shooting protons (accumulated in a proton storage ring) on a target material where pions are the most abundant secondary particles. The most effective pion production mechanism proceeds via decays of resonances. For pions it is dominated by the Δ_{33} isobar ($\Delta_{33} \to N\pi$) [basic processes $p+p \to p+n+\pi^+$ and $p+n \to p+p+\pi^-$]

$$p + (N, Z) \to \Delta^* + X \to \text{“}(N+1, Z+1 \mp 1)\text{”} + \pi^\pm\,,$$

where the ratio $\sigma(\pi^+)/\sigma(\pi^-) \to 1$ at high Z.[8]

---

[7] Only the recently established phenomenon of neutrino oscillations proves that lepton number in fact is not a perfect quantum number. This requires that neutrinos must have tiny masses and this requires that right–handed neutrinos (ν_R's) must exist. In fact, the smallness of the neutrino masses explains the strong suppression of lepton number violating effects.

[8] At Brookhaven the 24 GeV proton beam extracted from the AGS with 60×10^{12} protons per AGS cycle of 2.5 s impinges on a Nickel target of one interaction length and produces amongst other debris–particles a large number of low energy pions. The pions are momentum selected and then decay in a straight section where about one third of the pions decay into muons. The latter are momentum selected once more before they are injected into the $g-2$ storage ring.

We now look more closely to the decay chain

$$\begin{aligned}\pi &\to \mu + \nu_\mu \\ &\quad \hookrightarrow\ e + \nu_e + \nu_\mu\,,\end{aligned}$$

producing the polarized muons which decay into electrons which carry along in their direction of propagation the knowledge of the muon's polarization (for a detailed discussion see e.g. [34]).

(1) Pion decay:

The π^- is a pseudoscalar bound state $\pi^- = (\bar{u}\gamma_5 d)$ of a d quark and a u antiquark $\bar{u}$. The main decay channel is via the diagram:

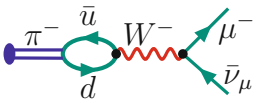

π–decay

In this two–body decay of the charged spin zero pseudoscalar mesons the lepton energy is fixed (monochromatic) and given by

$$E_\ell = \sqrt{m_\ell^2 + p_\ell^2} = \frac{m_\pi^2 + m_\ell^2}{2m_\pi}\,,\quad p_\ell = \frac{m_\pi^2 - m_\ell^2}{2m_\pi}\,.$$

Here the relevant part of the Fermi type effective Lagrangian reads

$$\mathcal{L}_{\text{eff,int}} = -\frac{G_\mu}{\sqrt{2}}\, V_{ud}\, \left(\bar{\mu}\gamma^\alpha\,(1-\gamma_5)\,\nu_\mu\right)\left(\bar{u}\gamma_\alpha\,(1-\gamma_5)\,d\right) + \text{h.c.}\,,$$

where G_μ denotes the Fermi constant and V_{ud} the first entry in the CKM matrix. For our purpose $V_{ud} \sim 1$. The transition matrix–element reads

$$\begin{aligned}T &= {}_{\text{out}}\!<\mu^-, \bar{\nu}_\mu|\pi^->_{\text{in}} \\ &= -\text{i}\frac{G_\mu}{\sqrt{2}}\, V_{ud}\, F_\pi\, \left(\bar{u}_\mu\gamma^\alpha\,(1-\gamma_5)\,v_{\nu_\mu}\right)\, p_\alpha\,,\end{aligned}$$

where we used the hadronic matrix–element

$$\left\langle 0|\,\bar{d}\,\gamma_\mu\gamma_5\,u\,|\pi(p)\right\rangle \doteq \text{i}F_\pi p_\mu\,,$$

which defines the pion decay constant F_π. As we know the pion is a pseudoscalar such that only the axial part of the weak charged $V-A$ current couples to the pion. By angular momentum conservation, as the π^+ has spin 0 and the emitted neutrino is left–handed ($(1-\gamma_5)/2$ projector) the μ^+ must be left–handed as well. Going to the

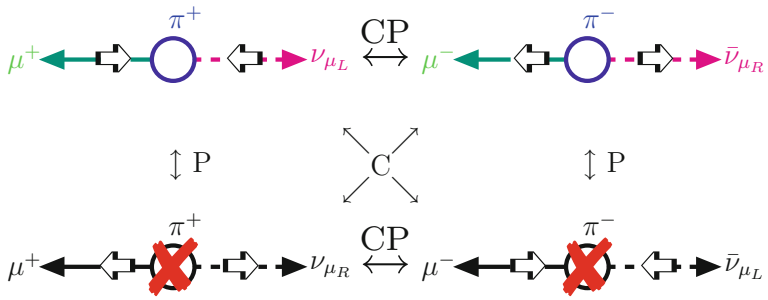

Fig. 6.9 Pion decay is a parity violating weak decay where leptons of definite handedness are produced depending on the given charge. CP is conserved while P and C are violated maximally (unique handedness). μ^- [μ^+] is produced with positive [negative] helicity $h = \mathbf{S} \cdot \mathbf{p}/|\mathbf{p}|$. The existing μ^- and μ^+ decays are related by a CP transformation. The decays obtained by C or P alone are nonexistent in nature

π^- not only particles have to be replaced by antiparticles (C) but also the helicities have to be reversed (P), since a left–handed antineutrino (essentially) does not exist. Note that the decay is possible only due to the non–zero muon mass, which allows for the necessary helicity flip of the muon. The handedness is opposite for the opposite charge. This is illustrated in Fig. 6.9.

The pion decay rate is given by

$$\Gamma_{\pi^- \to \mu^- \bar{\nu}_\mu} = \frac{G_\mu^2}{8\pi} |V_{ud}|^2 F_\pi^2 \, m_\pi \, m_\mu^2 \left(1 - \frac{m_\mu^2}{m_\pi^2}\right)^2 \times \left(1 + \delta_{\text{QED}}\right) \,,$$

with CKM matrix–element $V_{ud} \sim 1$ and δ_{QED} the electromagnetic correction.

(2) Muon decay:

Muon decay $\mu^- \to e^- \bar{\nu}_e \nu_\mu$ is a three body decay

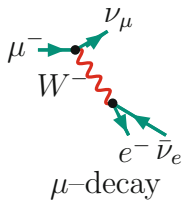

μ–decay

The matrix element can be easily calculated. The relevant part of the effective Lagrangian reads

$$\mathcal{L}_{\text{eff,int}} = -\frac{G_\mu}{\sqrt{2}} \left(\bar{e}\gamma^\alpha \left(1 - \gamma_5\right) \nu_e\right) \left(\bar{\nu}_\mu \gamma_\alpha \left(1 - \gamma_5\right) \mu\right) + \text{h.c.} \,,$$

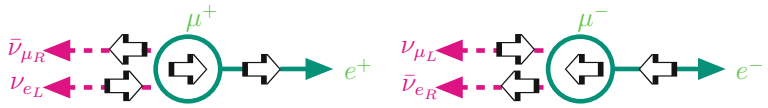

Fig. 6.10 In μ^- [μ^+] decay the produced e^- [e^+] has negative [positive] helicity, respectively

and thus

$$\begin{aligned} T &= {}_{\text{out}}\!<e^-, \bar{\nu}_e \nu_\mu | \mu^- >_{\text{in}} \\ &= \frac{G_\mu}{\sqrt{2}} \left(\bar{u}_e \gamma^\alpha \left(1-\gamma_5\right) v_{\nu_e}\right) \left(\bar{u}_{\nu_\mu} \gamma_\alpha \left(1-\gamma_5\right) u_\mu\right) , \end{aligned}$$

which proves that the μ^- and the e^- have both the same left–handed helicity [the corresponding anti–particles are right–handed] in the massless approximation. This implies the decay scheme Fig. 6.10 for the muon.

The positrons are thus emitted preferably in the direction of the muon spin, and measuring the direction of the positron momentum provides the direction of the muon spin.

After integrating out the two unobservable neutrinos, the polarized differential decay probability to find an $e^\pm$ with energy between E_e and $E_e + \mathrm{d}E_e$ emitted at an angle between θ and $\theta + \mathrm{d}\theta$ reads (see also (2.47))

$$\frac{\mathrm{d}^2\Gamma}{\mathrm{d}E_e \mathrm{d}\cos\theta} = \frac{G_\mu^2}{12\pi^3} \frac{p_e}{E_\mu} \left\{ Q^2 \left(p_0 p_1\right) + 2 \left(Q p_0\right) \left(Q p_1\right) - \left(n_0 p_1\right) \left(Q^2 - 2 \left(Q p_1\right)\right) \right\} , \quad (6.56)$$

with p_0 the muon momentum, p_1 the positron/electron momentum, n_0 the muon polarization vector $n_0^2 = -1$, $n_0 p_0 = 0$ ($n_0 = (0, \mathbf{P}_\mu)$ in the muon rest frame) where $Q = p_0 - p_1$, $Q^2 = m_\mu^2 + m_e^2 - 2\left(p_0 p_1\right)$. For a polarized muon $P_\mu = |\mathbf{P}_\mu| = 1$, in practice $P_\mu < 1$ describes the degree of polarization. As $(n_0 p_1)$ is L-invariant, its value is as given in the muon rest frame[9]: $(n_0 p_1) = -P_\mu \sqrt{E_e^2 - m e^2}\, \cos\theta$. The asymmetry proportional to the coefficient of $(n p_0)$

$$A \propto \frac{\left(Q^2 - 2 \left(Q p_1\right)\right)}{Q^2 \left(p_0 p_1\right) + 2 \left(Q p_0\right) \left(Q p_1\right)}$$

[9]Note that the original electron phase space element $\mathrm{d}V_e \equiv \frac{\mathrm{d}^3 p_1}{E_e}$ is L–invariant such that with $\mathrm{d}^3 p_1 = -p_e^2 \mathrm{d}p_e\, \mathrm{d}\cos\theta\, \mathrm{d}\varphi$, after integrating over the azimuthal angle φ, giving a factor 2π, and using $p_e \mathrm{d}p_e = E_e \mathrm{d}E_e$ we infer that $\mathrm{d}V_e \to 2\pi \sqrt{E_e^2 - m_e^2}\, \mathrm{d}E_e\, \mathrm{d}\cos\theta$ is independent of the frame. While in the rest frame $u_0 p_1 = -\mathbf{P}_\mu \mathbf{p}_1 = -P_\mu p_e \cos\theta$ in the laboratory frame $u_0 = \left(1, \frac{\mathbf{p}_0}{E_0 - m}\right) \frac{\mathbf{p}_0 \mathbf{P}_\mu}{m}$ and thus $u_0 p_1 = \cos\theta_\mu \frac{p_\mu}{m} \left(E_e - \frac{p_\mu p_{1x}}{E_0 - m}\right)$.

is also independent of the frame. In the muon rest frame, in terms of the fractional positron/electron energy $x = E_e/W$ and $x_0 = m_e/W$ where $W = \max E_e = (m_\mu^2 + m_e^2)/2m_\mu$ we have[10]

$$\frac{\mathrm{d}^2\Gamma^\pm}{\mathrm{d}x\,\mathrm{d}\cos\theta} = \frac{G_\mu^2 m_\mu^5}{96\pi^3}\left(1+\frac{m_e^2}{m_\mu^2}\right)^4 \sqrt{x^2-x_0^2}\left\{(3x-2x^2-x_0^2) \pm P_\mu\sqrt{x^2-x_0^2}\left(2x-1-x_0\frac{m_e}{m_\mu}\right)\cos\theta\right\},$$

or neglecting the electron mass

$$\frac{d^2\Gamma^\pm}{\mathrm{d}x\,d\cos\theta} = \frac{G_\mu^2 m_\mu^5}{192\pi^3}\,x^2\,\left(3-2x \pm P_\mu\,(2x-1)\,\cos\theta\right)\,. \tag{6.57}$$

Typically, the μ–decay spectrum is strongly peaked at small angles θ, the $e^\pm$ emission angle between the e momentum $\mathbf{p}_e$ and the muon polarization vector $\mathbf{P}_\mu$. The result above holds in the approximation $x_0 = m_e/W \sim 9.67\times10^{-3} \simeq 0$.

Assuming unit polarization, the $\mu^\pm$ decay spectrum may be written in the form Eq. (6.3) discussed earlier or equivalently

$$\begin{aligned} W^\pm(x,\cos\theta)\,\mathrm{d}x\,\mathrm{d}\cos\theta &= \tau_\mu^{-1}\,x^2\,(3-2x)\left[1\pm\frac{2x-1}{3-2x}\,\cos\theta\right] \\ &= \tau_\mu^{-1}\,\frac{N(E_e)}{2}\,[1+A(E_e)\,\cos\theta]\,\mathrm{d}x\,\mathrm{d}\cos\theta\,, \end{aligned}$$

where

$$N(E_e) = 2x^2(3-2x)\;,\quad \left[\int_0^1 \mathrm{d}x N(x) = 1\right]\,, \tag{6.58}$$

represents a normalizing spectrum and

$$A(E_e) = \frac{2\,x-1}{3-2\,x}\;,\quad \left[\int_0^1 \mathrm{d}x N(x)A(x) = 1/3\right]\,, \tag{6.59}$$

is the asymmetry which reflects the *parity violation* and strongly correlates the muon spin with the positron momentum direction. The asymmetry changes sign at $x = 1/2$.

Figure 6.11 shows energy spectrum $N(x)$) as a function of x where the positron energy from the normal $\mu^\pm$–decay is $E_e = x\times 52.83\,\mathrm{MeV}$. $A(E_e)$ is the $e^\pm$ energy dependent $\mu^\pm$–decay asymmetry, the degree of correlation between $e^\pm$ momentum and $\mu^\pm$ spin direction. For the μ^- decay $A(E_e)$ has the opposite sign. Also displayed is the weighted μ^+ decay asymmetry spectrum, the product of N and A^2. The average asymmetry is

[10] With $Q^2{=}m_\mu^2 + m_e^2 - 2p_0p_1$, $Qp_0{=}m_\mu^2 - p_0p_1$, $Qp_1{=}p_0p_1 - m_e^2$, and $p_0p_1{=}m_\mu E_e$, $E_e = xW$, $m_\mu = 2W$ the curly bracket of (6.56) reads $\{\cdots\} = 8W^4\,x\,\left[(3-2x) + P_\mu\cos\theta\,(2x-1)\right] + O(m_e^2/m_\mu^2)$.

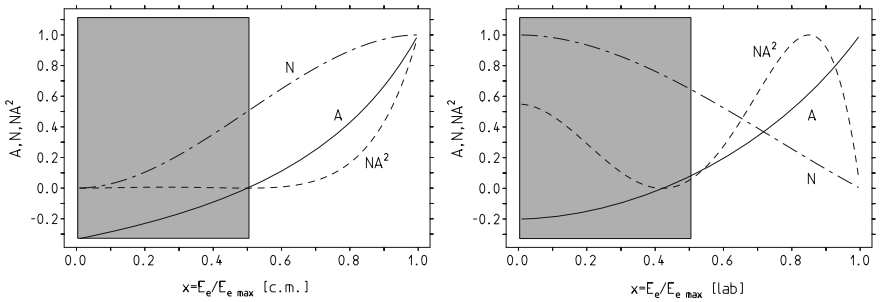

Fig. 6.11 Number of decay positrons per unit energy (Michel spectrum) N (arbitrary units), value of the asymmetry A, and relative yield NA^2 (arbitrary units) as a function of the positron energy in units of the maximal positron energy. The polarization is assumed to be unity. Events in the shaded region $E < E_{\rm th}$ are not counted, since if all events are integrated the asymmetry gets largely canceled. *Left* as seen in the muon rest frame. *Right* as seen in the laboratory frame

$$A = \frac{\int_0^1 \mathrm{d}x N(x) A(x)}{\int_0^1 \mathrm{d}x N(x)} = \frac{1}{3} \; ; \quad \frac{W(\cos\theta)}{\mathrm{d}\cos\theta} = \frac{1}{2}\left(1 + A\,\cos\theta\right) = \frac{1}{2}\left(1 + \frac{1}{3}\,\cos\theta\right) \; .$$

What we see in the laboratory frame we obtain by the transformation (see [2])

$$E'_e = \gamma\,(E_e + \beta p_{ex}) \; ; \quad p'_{ex} = \gamma\,(p_{ex} + \beta E_e) \; , \quad p'_{ey} = p_{ey} \; , \quad p'_{ez} = p_{ez} \; ,$$

where $\gamma = E/m$ and $\beta = p/E$ when $p'_\mu = p^{\rm lab}_\mu = (E, p, 0, 0)$ boosted along the x–axis. Denoting θ' the positron emission angle in the laboratory frame, where the muon's spin precesses relative to the momentum vector such that one can identify

$$\cos\theta' \to \cos\left(\omega_a\, t + \phi\right) \; ,$$

up to a phase ϕ. Adopting polar coordinates (x, θ_μ, φ) in the rest frame with $\mathbf{p}_\mu$ as a x–axis and $\varphi = 0$ in the plane of the muon spin precession, then, if the spin is at angle $(\omega_a\, t)$ to the muon direction, then it is at angle θ (introduced above) with respect to the positron direction. In terms of (θ_μ, φ)

$$\cos\theta = \cos\theta_\mu \cos(\omega_a t) + \sin\theta_\mu \sin(\omega_a t)\cos\varphi \; ,$$

and integrating over those positrons emitted within a region R in the muon rest frame which can be detected in the laboratory frame we have

$$\begin{aligned} &\frac{1}{2\pi}\int_R 2\tau_\mu\, W(x, \cos\theta)\,\mathrm{d}x\,\mathrm{d}\cos\theta\,\mathrm{d}\varphi \\ &= \frac{1}{2\pi}\int_R 2x^2\,(3-2x) + 2x^2\,(2x-1)\,\left[\cos\theta_\mu\cos(\omega_a\,t) + \sin\theta_\mu \sin(\omega_a\,t)\cos\varphi\right]\mathrm{d}x\,\mathrm{d}\cos\theta\,\mathrm{d}\varphi \; . \end{aligned}$$

Integrating over φ the second term in the square bracket vanishes, while the first gets a factor 2π, such that

$$N'_e = \int_x \int_{\cos\theta} 2x^2\,(3-2x)\,\mathrm{d}x\,\mathrm{d}\cos\theta\;;\quad N'_e A'_e = \int_x \int_{\cos\theta} 2x^2\,(2x-1)\,\cos\theta\,\mathrm{d}x\,\mathrm{d}\cos\theta\;.$$

What is the range R in $(x, \cos\theta)$ space which gets mapped to the positrons detected in the laboratory frame? In the laboratory frame the positron energy in units of $W \approx m_\mu/2$ takes values

$$x'_L = x\,\gamma_\mu\,\left(1+\cos\theta_\mu\right)\;,\quad x'_T = x\,\sin\theta_\mu\;,$$

where x'_L is the positron momentum along the boost direction and x'_T the one transverse to it. A **threshold energy** in the laboratory system fixes a lower bound for $x'^2_L + x'^2_T = x'^2_{\rm th}$ such that

$$x^2\,\gamma_\mu^2\,\left(1+\cos\theta_\mu\right)^2 + x^2\,\sin^2\theta_\mu \geq x'^2_{\rm th}$$

together with $x \leq 1$. Since $\gamma_\mu \gg 1$ we may neglect the transversal term and get

$$\cos\theta_\mu \geq x'{\rm th}/x\gamma_\mu - 1\;.$$

For $\cos\theta = 1 = x'_{\rm th}/x_{\rm min}\gamma_\mu - 1$ thus $1 \geq x \geq b/2$ where $b = x'_{\rm th}/\gamma_\mu$. Thus with $\int_{b/x}^1 \mathrm{d}\cos\theta = 2 - b/x$ and $\int_{b/x}^1 \cos\theta\,\mathrm{d}\cos\theta = b/x - b^2/2x^2$ and integrating $\int_{b/2}^1 \mathrm{d}x\cdots$ we obtain

$$N'_e = \left[2 - \frac{5b}{3} + \frac{b^3}{4} - \frac{b^4}{24}\right]\;;\quad N'_e A'_e = \left[\frac{b}{3} - \frac{b^3}{4} + \frac{b^4}{12}\right]\;,$$

where $b/2 \leq 1$. If we substitute $b = 2x_{\rm th}$ and drop an overall factor $2/3$ we obtain [1]

$$N'_e = (x_{\rm th}-1)^2\left(3 + x_{\rm th} - x_{\rm th}^2\right)\;;\quad N'_e A'_e = x_{\rm th}\,(2x_{\rm th}+1)\,(x_{\rm th}-1)^2\;. \quad (6.60)$$

The above result may be obtained as an integral $I(x_{\rm th}) = \int_{x_{\rm th}}^1 \mathrm{d}x\cdots$ by taking the derivative $-\mathrm{d}I(x_{\rm th})/\mathrm{d}x_{\rm th}$ which yields

$$A(E) = P_\mu\,\frac{1 + x' - 8x'^2}{4x'^2 - 5x' - 5}\;;\quad N(E) \propto (x'-1)(4x'^2 - 5x' - 5)$$

with $x' = E/E_{\max}$, E the positron's laboratory energy and $E_{\max} = 3.098\,\text{GeV}$. These equations correspond to the laboratory frame versions of (6.58) and (6.59).[11] Again, the positron number oscillation with time as a function of positron energy reads

$$N(t, E) = N_0(E)\, \mathrm{e}^{-t/\gamma\tau}\, [1 + A(E)\, \cos(\omega_a t + \phi(E))]\ ,$$

which we have plotted in the right panel of Fig. 6.11. The phase ϕ comes from the initial spin polarization of the muons. By plotting the number of decay positrons observed as a function of time, one may extract ω_a by fitting the data to the simple 5–parameter function (6.62) below. Since the determination of ω_a is based on the number of counts, there is a statistical uncertainty on ω_a. In fitting N_0, τ, ω_a and ϕ from $N(t)$, data–fitting statistics implies that the statistical error on ω_a is approximately [1]

$$\frac{\delta\omega_a}{\omega_a} \approx \frac{\sqrt{2}}{\omega_a\, \gamma\tau\, A\langle P\rangle\sqrt{N}}\ . \tag{6.61}$$

The factor $1/\sqrt{N}$ is statistical error of the data sample, the factor $1/A$ is obvious from $N^{-1}\delta N/\delta\omega_a \propto A$ and the factor $1/\omega_a\gamma\tau$ accounts for improvement of the accuracy with the number of oscillations per decay–time $\omega_a t/\frac{t}{\gamma\tau} = \omega_a\gamma\tau$. Also the average degree of the polarization $\langle P\rangle$ matters of course.The factor of $\sqrt{2}$ comes from the strong correlation between the phase ϕ and the frequency ω_a. Since both A and N depend on the energy-threshold and since one wishes to minimize the statistical uncertainty of ω_a, the energy-threshold is chosen such that the product NA^2 is maximized. Then counting all positrons above a threshold energy E_{th} the oscillation profile reads

$$N(t, E_{\text{th}}) = N_0(E_{\text{th}})\, \mathrm{e}^{-t/\gamma\tau}\, [1 + A(E_{\text{th}})\, \cos\,(\omega_a\, t + \phi(E_{\text{th}}))]\ , \tag{6.62}$$

with (using (6.60))

$$A(E_{\text{th}}) = P_\mu\, \frac{x_{\text{th}}\,(2x_{\text{th}} - 1)}{3 + x_{\text{th}} - x_{\text{th}}^2}\ ;\quad N(E_{\text{th}}) \propto (x_{\text{th}} - 1)^2(3 + x_{\text{th}} - x_{\text{th}}^2)\ .$$

Figure 6.12 shows that the "figure of merit" NA^2 has a maximum at $x_{\text{th}} \approx 0.65$, which corresponds to about 2 GeV. Equation (6.62) represents the actual time structure which is confronted with the experimental data to extract the Larmor precession angular frequency ω_a.

[11] Note that, this is not what one gets by writing (6.56) in terms of laboratory system variables. It is rather a matter of how the geometrical acceptance of the decay positrons/electrons is affected by boosting the system.

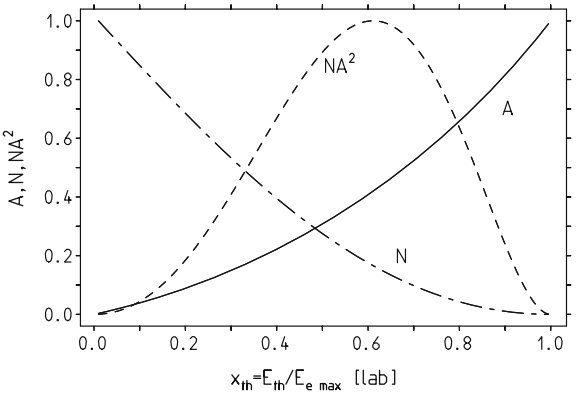

Fig. 6.12 Optimizing the quality $NA^2(E_{\text{th}})$ by an appropriate choice of the laboratory energy threshold E_{th} above which positrons/electrons are registered (see [1])

6.5 Muon $g-2$ Results

First a historical note: before the E821 experiment at Brookhaven the last of a series of measurement of the anomalous g-factor $a_\mu = (g_\mu - 2)/2$ at CERN was published about 30 years earlier. At that time a_μ had been measured for muons of both charges in the Muon Storage Ring at CERN. The two results,

$$\begin{aligned} a_{\mu^-} &= 1165937(12) \times 10^{-9} \,, \\ a_{\mu^+} &= 1165911(11) \times 10^{-9} \,, \end{aligned} \tag{6.63}$$

are in good agreement with each other, and combine to give a mean

$$a_\mu = 1165924.0(8.5)10^{-9} \;\; [7\,\text{ppm}] \,, \tag{6.64}$$

which was very close to the theoretical prediction $1165921.0(8.3)10^{-9}$ at that time. The measurements thus confirmed the remarkable QED calculation plus hadronic contribution, and served as a precise verification of the CPT theorem for muons.

Measured in the experiments is the ratio $R = \omega_a/\omega_p$ of the muon precession frequency $\omega_a = \omega_s - \omega_c$ and the proton precession frequency ω_p, which together with the ratio of the magnetic moment of the muon to the one of the proton $\lambda = \mu_\mu/\mu_p$ determines the anomalous magnetic moment as

$$a_\mu = \frac{R}{\lambda - R} \,. \tag{6.65}$$

The CERN determination of a_μ utilized the value $\lambda = 3.1833437(23)$.

The BNL muon $g-2$ experiment has been able to improve and perfect the method of the last CERN experiments in several respects and was able to achieve an impressive 14–fold improvement in precision. The measurements are $R_{\mu^-} = 0.0037072083(26)$ and $R_{\mu^+} = 0.0037072048(25)$ the difference being $\Delta R = (3.5 \pm$

Table 6.2 Summary of CERN and E821 results

Experiment	Year	Polarity	$a_\mu \times 10^{10}$	Precision [ppm]	References
CERN I	1961	μ^+	11 450 000 (220000)	4300	[35]
CERN II	1962–1968	μ^+	11 661 600 (3100)	270	[36]
CERN III	1974–1976	μ^+	11 659 100 (110)	10	[15]
CERN III	1975–1976	μ^-	11 659 360 (120)	10	[15]
BNL	1997	μ^+	11 659 251 (150)	13	[20]
BNL	1998	μ^+	11 659 191 (59)	5	[21]
BNL	1999	μ^+	11 659 202 (15)	1.3	[22]
BNL	2000	μ^+	11 659 204 (9)	0.73	[23]
BNL	2001	μ^-	11 659 214 (9)	0.72	[24]
	Average		11 659 208.0 (6.3)	0.54	[24]

$3.4) \times 10^{-9}$. Together with the updated muon-to-proton magnetic ratio[12] $\lambda = 3.183345107(84)$ [37] one obtains the new values

$$\begin{aligned} a_{\mu^-} &= 11659215(8)(3) \times 10^{-10} \,, \\ a_{\mu^+} &= 11659204(6)(5) \times 10^{-10} \,. \end{aligned} \tag{6.66}$$

Assuming CPT symmetry, as valid in any QFT, and taking into account correlations between systematic errors between the various data sets the new average $R = 0.0037072064(20)$ is obtained. From this result together with the updated λ (6.9) one obtains the new average value

$$a_\mu = 11659209.1(5.4)(3.3)[6.3] \times 10^{-10} \,, \tag{6.67}$$

with a relative uncertainty of 0.54 ppm [16]. Where two uncertainties are given the first is statistical and the second systematic, otherwise the total error is given where statistical and systematic errors have been added in quadrature. In Table 6.2 all results from CERN and E821 are collected. The new average is completely dominated by the BNL results. The individual measurements are shown also in Fig. 6.13. The comparison with the theoretical result is devoted to the next section. The achieved improvement and a comparison of the sensitivity to various kinds of physics effects has been shown earlier in Fig. 3.8 at the end of Sect. 3.2.1.

The following two sections are addenda, one on the determination of λ in (6.65) and the other a sketch of the electron $g-2$ measurement technique.

[12] This value is replacing $\lambda = 3.18334539(10)$ used in [24].

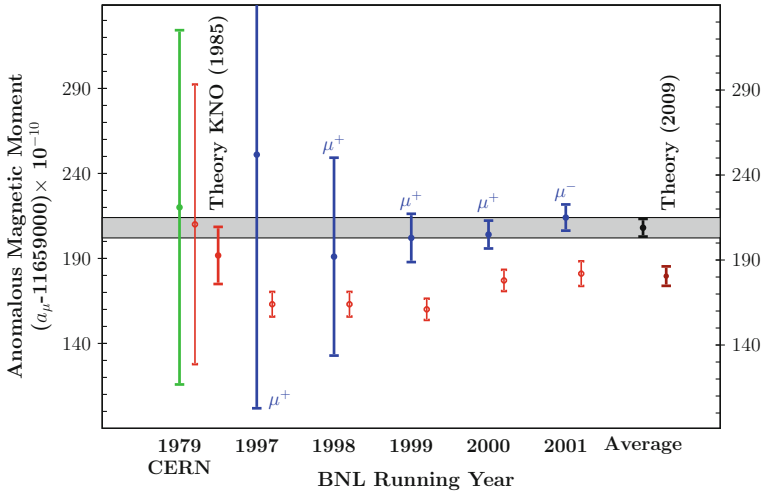

Fig. 6.13 Results for the individual E821 measurements, together with the new world average and the theoretical prediction. The CERN result is shown together with the theoretical prediction by Kinoshita et al. 1985, at about the time when the E821 project was proposed. The *dotted vertical bars* indicate the theory values quoted by the experiments

6.6 Ground State Hyperfine Structure of Muonium

The hyperfine and Zeeman levels of $^2S_{\frac{1}{2}}$ ground state Muonium are shown in Fig. 6.14. The energy levels are described by the Hamiltonian

$$\mathcal{H} = h\,\Delta\nu\,\mathbf{I}_\mu \cdot \mathbf{J} - \mu_{\mathrm{B}}^{\mu}\, g'_\mu\, \mathbf{I}_\mu \cdot \mathbf{B} + \mu_{\mathrm{B}}^{e}\, g_J\, \boldsymbol{J} \cdot \mathbf{B}\,, \tag{6.68}$$

where $\mathbf{I}_\mu$ is the muon spin operator, $\mathbf{J}$ is the electron total angular momentum operator and $\mathbf{B}$ is the external static magnetic field. The total angular momentum is $\mathbf{F} = \mathbf{J} + \mathbf{I}_\mu$.

Microwave transitions ν_{12} and ν_{34} are measured in a strong magnetic field B of 1.6 T. Also this experiment uses the parity violating correlation of the direction of the muon spin and the positron emission of μ–decay.

The hyperfine splitting (HFS) and the muon magnetic moment are determined from ν_{12} and ν_{34}.

$$\begin{aligned}
\nu_{12} &= -\mu_\mu B + \frac{\Delta\nu}{2}\left[1 + x - \sqrt{1+x^2}\right], \\
\nu_{34} &= +\mu_\mu B + \frac{\Delta\nu}{2}\left[1 - x + \sqrt{1+x^2}\right],
\end{aligned} \tag{6.69}$$

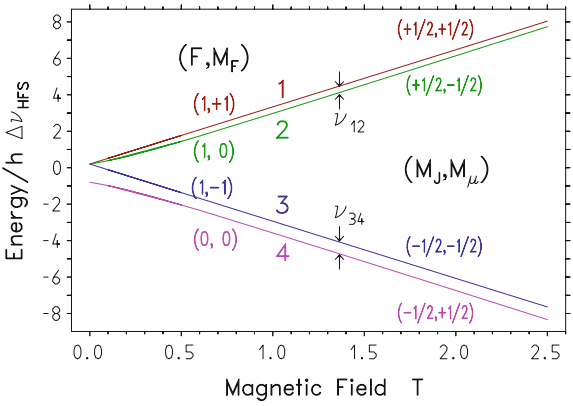

Fig. 6.14 Muonium ground state hyperfine structure Zeeman splitting (Breit-Rabi energy level diagram). At high fields the transitions ν_{12} and ν_{34} are essentially muon spin flip transitions

where $x = (g_J \mu_B^e + g'_\mu \mu_B^\mu)\, B/(h\Delta\nu)$ is proportional to the magnetic field strength B.[13] The latest experiment at LAMPF at Los Alamos has measured these level splittings very accurately. The Larmor relation, $2\mu_p B = h\nu_p$, and NMR is used to determine B in terms of the free proton precession frequency ν_p and the proton magnetic moment μ_p. Using (6.69) and the measured transition frequencies ν_{12} and ν_{34} both $\Delta\nu$ and μ_μ/μ_p can be determined.

Note that the sum of (6.69) equals to the zero field splitting $\Delta\nu \equiv \Delta\nu_{\rm HFS}$ independent of the field B, while for high fields the difference measures the magnetic moment μ_μ:

$$\Delta\nu = \nu_{12} + \nu_{34}\ ,$$
$$\mu_\mu B = \nu_{34} - \nu_{12} - \Delta\nu\left(\sqrt{1+x^2} - x\right) \approx \nu_{34} - \nu_{12} - \frac{\Delta\nu}{2x}\ ,\quad (x \gg 1)\ .$$

The magnetic moment was measured to be

$$\mu_\mu/\mu_p = 3.183\,345\,24(37)\ (120\,\text{ppb})\ ,$$

which translates into a muon–electron mass ratio

$$m_\mu/m_e = \left(\frac{g_\mu}{2}\right)\left(\frac{\mu_p}{\mu_\mu}\right)\left(\frac{\mu_{\rm B}^e}{\mu_p}\right) = 206.768\,276(24)\ (120\,\text{ppb})\ ,$$

[13] The gyromagnetic ratios of the bound electron and muon differ from the free ones by the binding corrections [38]

$$g_J = g_e\left(1 - \frac{\alpha^2}{3} + \frac{\alpha^2}{2}\frac{m_e}{m_\mu} + \frac{\alpha^3}{4\pi}\right)\ ,\quad g'_\mu = g_\mu\left(1 - \frac{\alpha^2}{3} + \frac{\alpha^2}{2}\frac{m_e}{m_\mu}\right)\ .$$

.

when using $g_\mu = 2\,(1 + a_\mu)$ with $a_\mu = 11\,659\,208.0(6.3) \times 10^{-10}$ and $\mu_p/\mu_B^e = 1.521\,032\,206(15) \times 10^{-3}$ [30]. The measured value of the zero field HFS is

$$\Delta\nu^{\text{exp}} = 4\,463\,302\,765(53)\ \text{Hz}\ (12\,\text{ppb})\,,$$

in good agreement with the theoretical prediction [27, 28, 30, 39–41]

$$\begin{aligned}\Delta\nu^{\text{the}} &= \frac{16}{3}\,c\,R_\infty\,\alpha^2\,\frac{m_e}{m_\mu}\left(1+\frac{m_e}{m_\mu}\right)^{-3}\left(1+\delta\mathcal{F}(\alpha, m_e/m_\mu)\right)\\ &= 4\,463\,302\,905(272)\ \text{Hz}\ (61\,\text{ppb})\,,\end{aligned}$$

where the error is mainly due to the uncertainty in m_μ/m_e. The correction $\delta\mathcal{F}(\alpha, m_e/m_\mu)$ depends weakly on α and m_e/m_μ,

$$R_\infty = 10\,973\,731.568\,525(37)\ \text{m}^{-1}$$

is the Rydberg constant $\alpha^2 m_e c/2h$ [30]. A combined result was used to determine (6.9) used in the determination of a_μ (see also [42]).

6.7 Single Electron Dynamics and the Electron $g - 2$

The basic principle of a muon $g - 2$ experiment is in many respects very similar to the one of electron $g - 2$ experiments, although the scale of the experiment is very different and the electron $g - 2$ experiment uses atomic spectroscopy type methods to determine the frequencies. The particle dynamics considered in Sect. 6.2 applies to the single electron or single ion Penning trap shown in Fig. 6.15. Electron motion in a hyperboloid Penning trap in the *axial* (vertical) direction is a harmonic oscillation

$$z(t) = A\cos(\omega_z t)\,,$$

with

$$\omega_z = 2\sqrt{eV_0/md^2}\,,$$

(see (6.15)). In the *radial* direction it is an epicycloid motion with

$$\begin{aligned}x(t) &= +\rho_m\cos(\omega_m t) + \rho_c\cos(\omega_c' t)\,,\\ y(t) &= -\rho_m\sin(\omega_m t) - \rho_c\sin(\omega_c' t)\,.\end{aligned}$$

Here

$$\omega_c' = \omega_+ = \frac{1}{2}(\omega_c + \sqrt{\omega_c^2 - 2\omega_z^2}\,) \simeq \omega_c$$

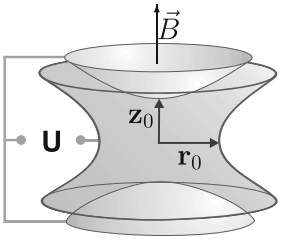

(a) Penning trap: an electrical quadrupole field superimposed on a homogeneous magnetic field ($U = V_0$)

(b) Penning trap device (in units of the size of a 1 € coin)

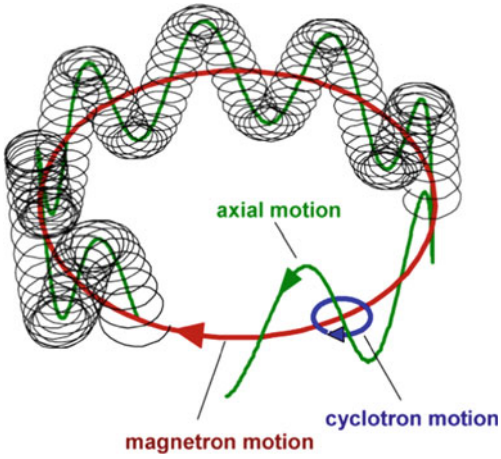

(c) Typical electron trajectory

Fig. 6.15 Electron motion in a hyperbolic Penning trap Courtesy of G. Werth, Mainz [43]

is the *perturbed cyclotron frequency* and

$$\omega_m = \omega_- = \frac{1}{2}(\omega_c - \sqrt{\omega_c^2 - 2\omega_z^2}) = \omega_c - \omega_c'$$

the *magnetron frequency*. The frequencies are related by $\omega_c^2 = \omega_+^2 + \omega_-^2 + \omega_z^2$. Typical values for a positron in a magnetic field $B = 3\,\mathrm{T}$, $U = 10\,\mathrm{V}$ and $d = 3.3\,\mathrm{mm}$ are $\nu_c = 48\,\mathrm{GHz}$, $\nu_z = 64\,\mathrm{MHz}$, $\nu_m = 12\,\mathrm{kHz}$ depending on the field strengths determined by B, U and d.

The observation of the splitting of the spin states requires a coupling of the cyclotron and spin motion of the trapped electron to the axial oscillation, which is realized by an extremely weak magnetic bottle modifying the uniform magnetic field by an inhomogeneous component (Dehmelt et al. [44]) (see Fig. 6.16). The latter is imposed by a ferromagnetic ring electrode, such that

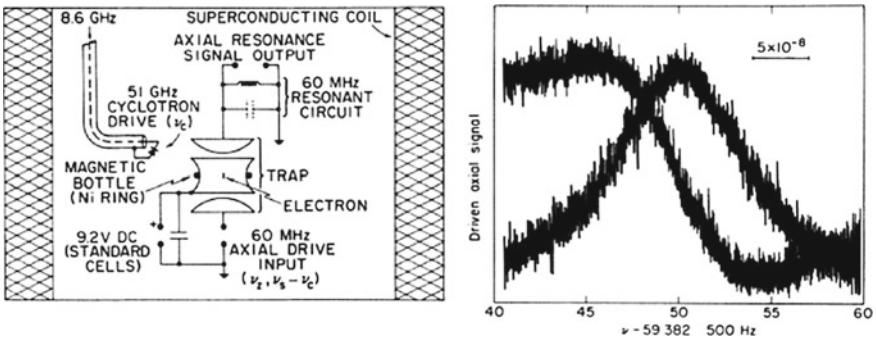

Fig. 6.16 *Left* schematic of the geonium apparatus (Dehmelt et al. [44]). Hyperbolic end caps and ring electrodes trap the electron axially while coupling the driven harmonic motion to an external LC circuit tuned to drive the axial frequency. Radial trapping of the electron is produced by the strong magnetic field from a superconducting solenoid. *Right* frequency shift in the axial resonance signal at ≈60 MHz. The signal–to–noise ratio of this ≈8 Hz wide line corresponds to a frequency resolution of 10 ppb. Reprinted with permission from [44]. Copyright (2007) by the American Physical Society

$$B = B_0 + B_2\, z^2 + \cdots\,, \tag{6.70}$$

which imposes a force

$$F = m_s\, g_e\, \mu_B\, \text{grad}\, B = m_s\, g_e\, \mu_B\, B_2\, z$$

on the magnetic moment. Because of the cylindrical symmetry the force is linear in first order and the motion remains harmonic. The force adds or subtracts a component depending on $m_s = \pm 1/2$ and thus changes the axial frequency by

$$\Delta\omega_z = g_e\, \mu_B\, \frac{B_2}{m_e \omega_z}\,, \tag{6.71}$$

as shown in Fig. 6.16.

For a trap working at a temperature of $T = 4°$ K the thermic energy is $E = kT = 3.45 \times 10^{-4}$ eV. The trapped electron occupies low quantum states, the cyclotron ($n = 0, 1, 2, \ldots$) and spin ($m_s = \pm 1/2$) energy levels,

$$E(n, m_s) = \left(n + \frac{1}{2}\right) \hbar\omega_c' + \frac{g_e}{2}\, \hbar\omega_c\, m_s - \frac{h}{2}\delta \left(n + \frac{1}{2} + m_s\right)^2\,, \tag{6.72}$$

for $\nu_c = 84$ GHz thus $\hbar\omega_c = 3.47 \times 10^{-4}$ eV which implies $n_c = 0, 1$ such that QM is at work (the axial motion corresponds to $n_z \simeq 1000$ and hence is classical).

In fact this is not quite true: Gabrielse has shown that in Dehmelt's experiment at 4° K, because of the spread in the thermic spectrum, still many higher states are populated and, in a field of a few Tesla, only at about $T = 0.1°$ K one reaches the ground state [45]. The third term in (6.72) is the leading relativistic correction of

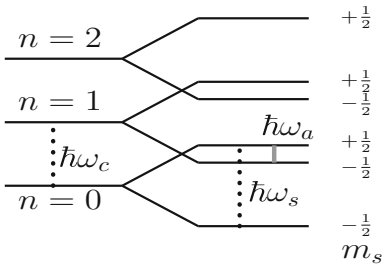

Fig. 6.17 Lowest electron quantum states in a Penning trap

size $\delta/\nu_c \equiv h\nu_c/(mc^2) \approx 10^{-9}$ [46], too small to be important at the present level of accuracy of the experiments. The radiation damping is

$$\frac{\mathrm{d}E}{\mathrm{d}t} = -\hat{\gamma}E\ ,\quad \hat{\gamma} = \frac{e^2\omega^2}{6\pi\epsilon_0 mc^3}\ , \tag{6.73}$$

and with $\alpha\hbar c = e^2/(4\pi\epsilon_0) = 1.44\,\mathrm{MeVfm}$ one has $\hat{\gamma}_c = 1.75\,\mathrm{s}^{-1}$. The spontaneous damping by radiation is then $\hat{\gamma}_z \simeq \hat{\gamma}_c/10^6 \simeq 0.15$ per day. The $g-2$ follows from the spin level splitting Fig. 6.17

$$\Delta E = g_e\,\mu_B\,B = \frac{g_e}{2}\hbar\omega_c \equiv \hbar\omega_s\ , \tag{6.74}$$

such that

$$a_e \equiv \frac{g_e-2}{2} = \frac{\omega_s-\omega_c}{\omega_c} \equiv \frac{\omega_a}{\omega_c}\ . \tag{6.75}$$

From the spin Larmor precession frequency $\hbar\omega_s = m_e\,g_e\,\mu_B\,B$ (μ_B the Bohr magneton) and the calibration of the magnetic field by the cyclotron frequency of a single ion in the Penning trap $\hbar\omega_c = q_{\mathrm{ion}}/M_{\mathrm{ion}}\,B$ one obtains

$$g_e = 2\,\frac{\omega_s}{\omega_c}\,\frac{q_{\mathrm{ion}}}{e}\,\frac{m_e}{M_{\mathrm{ion}}}\ , \tag{6.76}$$

or if g_e is assumed to be known one may determine the electron mass very precisely. The most precise determination was obtained from g-factor experiments on $^{12}C^{5+}$ and $^{16}C^{7+}$ [47] with a cylindrical cryogenic double Penning trap in a magnetic field of 3.8 T [working at frequencies $\nu_c = 25\,\mathrm{MHz}$, $\nu_z = 1\,\mathrm{MHz}$, $\nu_m = 16\,\mathrm{kHz}$].

The Harvard electron $g-2$ experiment [48, 49] performs spectroscopy of a single electron in the lowest cyclotron and spin levels in a cylindrical Penning trap (see Fig. 6.18). The problem of a harmonic Penning trap is that it is a cavity and hence allows only certain electromagnetic frequencies. The damping by spontaneous emission affects the cyclotron frequency in a way which is not fully under control. The cylindrical trap which exhibits plenty of higher harmonics solves this problem as it can be operated at well selected frequencies. Working frequencies are

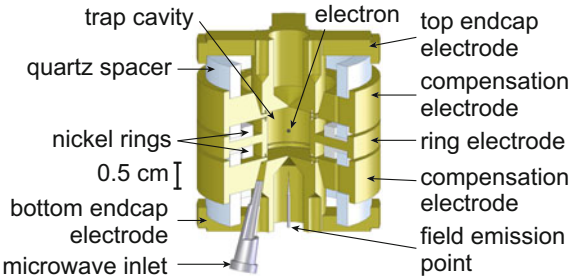

Fig. 6.18 Cylindrical Penning trap cavity used to confine a single electron and inhibit spontaneous emission. Reprinted with permission from [48]. Copyright (2008) by the American Physical Society, http://dx.doi.org/10.1103/PhysRevLett.100.120801

$\nu_s \approx \nu_c \approx 149\,\text{GHz}$, $\nu_z \approx 200\,\text{MHz}$, $\nu_m \approx$ 134kHz. For the first time it was possible to work with the lowest quantum states of (6.72) (see Fig. 6.17) in the determination of $g_e - 2$. The result has been discussed in Sect. 3.2.2.

6.8 The Upcoming Experiments: What Is New?

A new more precise experiment has to improve on the ingredients of (6.6) which more explicitly reads

$$a_\mu = \frac{\omega_a/\tilde{\omega}_p}{\mu_\mu/\mu_p - \omega_a/\tilde{\omega}_p}\,, \tag{6.77}$$

where ω_a is the muon spin precession frequency and $\tilde{\omega}_p$ the proton cyclotron frequency in the average magnetic field seen by the muons. Both frequencies will be provided by the new muon $g-2$ experiments. One ingredient, the μ_μ/μ_p ratio, which has been obtained with the muonium HFS experiment at LAMPF, will be limited at 120 ppb.

The Fermilab experiment [9–11] will improve the present error of a_μ from 540 to 140 ppb by a more precise determination of ω_a/ω_p. The principle of the experiment is the same as described earlier in this chapter. The improvements concern

- ω_a : one of the main issues at BNL was the limited statistics. At Fermilab highly intense shots of polarized 3.094 GeV/c muons will be available (21 times BNL), which will turn the formerly statistics dominated measurement into a systematics dominated one. The final data sample will include 1.5×10^{11} events in the final fit. This will give $\delta\omega_a(\text{statistics}) = 110$ ppb. The background from hadronic decays is eliminated as all pions decay and protons are removed from the muon beam before injection into the storage ring. Further improvements include:
  - new injection and kicker system (the frequency at BNL was disturbingly close to the second harmonic of ω_a, which affected the BNL analysis).
  - Improved systematics to 70 ppb concerning pileup, gain and energy scale stability and muon losses.
  - Improved correction for electric field and pitch, better control of the beam profile.

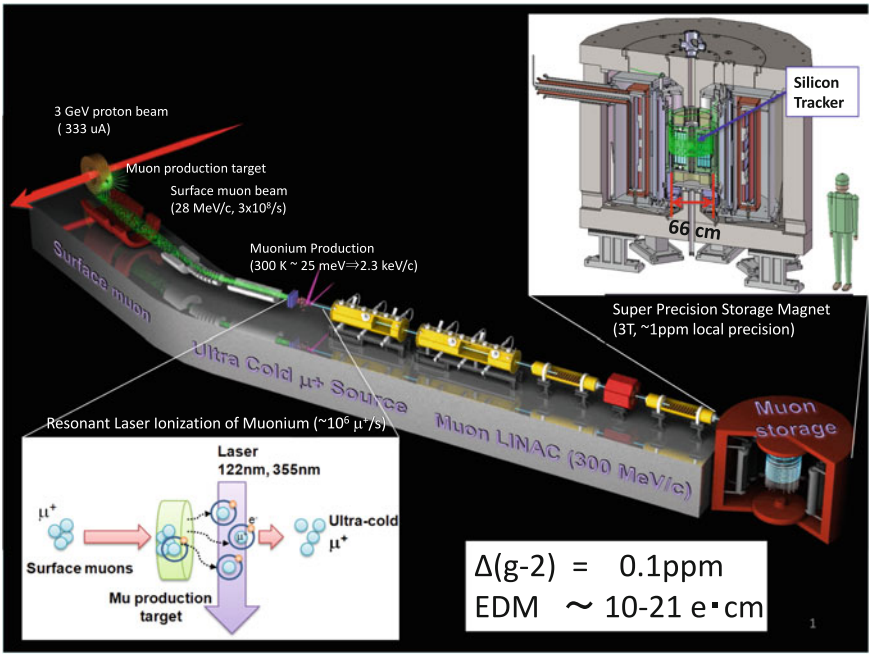

Fig. 6.19 Ultra-cold muon generation beam line and muon storage for the E34 experiment at J-PARC. Courtesy of the J-PARC g-2 Collaboration

- ω_p : better homogeneity and control/calibration of the homogeneous magnetic field i.e. improved $\tilde{\omega}_p$ at the 70 ppb level (factor 2 improvement over BNL).

The J-PARC experiment [12–14] planned to work with ultra cold muons represents a novel approach. Slow polarized muons are injected again into a homogeneous magnetic field filling a cylindrical trap free of any electrical fields. Thus the basic precession equation (6.2) again reduces to the simple $\omega_a = \frac{e}{m_\mu c}\, a_\mu\, B$ form. The size of the trap is almost a table top experiment. There is no electric beam focusing, meaning that muons need be injected at zero transverse momentum. The slow muons are living much shorter, by close to the factor $\gamma_{\text{magic}}/\gamma_{\text{cold}} \approx 10$ relative to the magic γ type experiments. However, muons are moving in a much smaller device. Smaller magnet fields intrinsically are more uniform. The principle is illustrated in Figs. 6.19 and 6.20. Data acquisition takes place within the small trap volume. The positron/electron number count again will be fitted to a function of the form (6.62). However, the completely different setup as a small low energy experiment implies rather different parameters in (6.62) and correspondingly in (6.61). On the one hand ω_a will be bigger because a bigger magnetic field will be applied, on the other hand $\gamma_{\text{magic}} \approx 30 \rightarrow \gamma_{\text{cold}} \approx 3$ such that $\gamma\tau$ appears reduced by a factor about 10 and is much smaller now. Also the degree of polarization expected to be about 50% (comparing to the expected 97% with E989) affects the statistical precision. The size

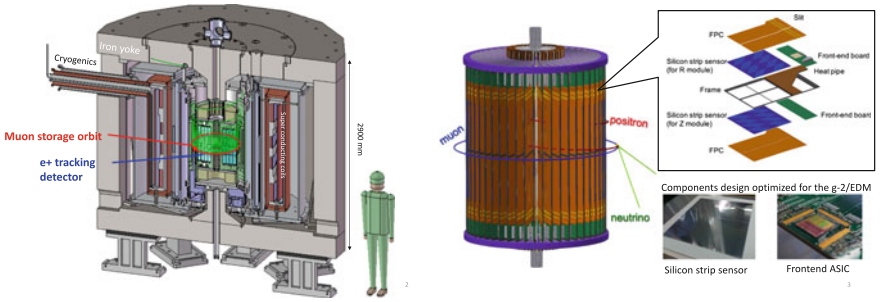

Fig. 6.20 *Left* magnet with storage ring and 3-dimensional spiral injection. *Right* Silicon tracker for positron detection. Courtesy of the J-PARC g-2 Collaboration. Private communication by T. Mibe

Table 6.3 Comparison of main parameters for the Fermilab and J-PARC $g-2$ experiments. The parameters of the Fermilab experiment are identical with the ones of the Brookhaven experiment (except from the statistics: BNL registered about 3.6×10^9 events, and had A = 0.3)

Parameter	Fermilab E989	J-PARC E34
Muon lab energy	3.098 GeV	300 MeV
Radius	7.11 m	33.3 cm
Cyclotron period	149.1 ns	7.4 ns
Lifetime, $\gamma\tau$	64.4 μs	6.6 μs
Effective asymmetry A	0.4	0.4
Beam polarization	0.97	0.50
Magnetic field	1.45 T	3.0 T
Precession frequency ω_a	1.43 MHz	2.96 MHz
Events in final fit	1.8×10^{11}	8.1×10^{11}
Statistical goal	140 ppb	400 ppb

of the effective asymmetry may be tuned to be comparable. In a first step the E34 experiment attempts to reach the precision of the BNL experiment. In Table 6.3 we compare the main parameters between the Fermilab/Brookhaven and the J-PARC experiments. While the E989 experiment is expected to substantiate the present 3 to 4 σ deviation as a new physics effect, the E43 experiment in a first step will scrutinize possible unaccounted systematic effects in the comparison between theory and experiment. We should keep in mind that the basic BMT equation (6.2) does not include possible higher order real photon radiation effects[14] which are very different for ultra relativistic and ultra cold muons.

[14]What I mean is that, as in Sect. 6.3, one solves the Dirac equation in en external field (the first of the QED field Eq. (3.1) with zero radiation field $A_\mu(x) \equiv 0$) rather than the coupled QED field equations.

References

1. J. Bailey et al., Nuovo Cim. A **9**, 369 (1972)
2. F. Combley, E. Picasso, Phys. Rep. **14C**, 1 (1974)
3. F.J.M. Farley, E. Picasso, in *Quantum Electrodynamics*, ed. by T. Kinoshita (World Scientific, Singapore 1990), p. 479; Adv. Ser. Direct. High Energy Phys. **7**, 479 (1990)
4. V.W. Hughes, The anomalous magnetic moment of the muon, in *International School of Subnuclear Physics: 39th Course: New Fields and Strings in Subnuclear Physics*, Erice, Italy, 29 Aug–7 Sep (2001); Int. J. Mod. Phys. A **18S1**, 215 (2003)
5. F.J.M. Farley, Y.K. Semertzidis, Prog. Part. Nucl. Phys. **52**, 1 (2004)
6. D.W. Hertzog, W.M. Morse, Annu. Rev. Nucl. Part. Sci. **54**, 141 (2004)
7. J.M. Paley, Measurement of the anomalous magnetic moment of the negative muon to 0.7 parts per million, Boston University Dissertation, 2004, Available from the UMI Thesis Server
8. J.P. Miller, E. de Rafael, B.L. Roberts, Rep. Prog. Phys. **70**, 795 (2007). doi:10.1088/0034-4885/70/5/R03
9. J. Grange et al. [Muon g-2 Collab.], arXiv:1501.06858 [physics.ins-det]
10. D.W. Hertzog, EPJ Web Conf. **118**, 01015 (2016). doi:10.1051/epjconf/201611801015
11. G. Venanzoni [Fermilab E989 Collab.], Nucl. Part. Phys. Proc. **273–275**, 584 (2016). doi:10.1016/j.nuclphysbps.2015.09.087; PoS EPS-HEP2015, 568 (2015)
12. N. Saito [J-PARC g-2/EDM Collab.], AIP Conf. Proc. **1467**, 45 (2012). doi:10.1063/1.4742078
13. H. Iinuma [J-PARC muon g-2/EDM Collab.], J. Phys. Conf. Ser. **295**, 012032 (2011). doi:10.1088/1742-6596/295/1/012032
14. T. Mibe [J-PARC g-2 Collab.], Nucl. Phys. Proc. Suppl. **218**, 242 (2011). doi:10.1016/j.nuclphysbps.2011.06.039
15. J. Bailey et al., Nucl. Phys. B **150**, 1 (1979)
16. G.W. Bennett et al. [Muon g-2 Collab.], Phys. Rev. D **73**, 072003 (2006)
17. G.T. Danby et al., Nucl. Instrum. Methods Phys. Res. A **457**, 151 (2001)
18. Y.K. Semertzidis, Nucl. Instrum. Methods Phys. Res. A **503**, 458 (2003)
19. E. Efstathiadis et al., Nucl. Instrum. Methods Phys. Res. A **496**, 8 (2002)
20. R.M. Carey et al., Phys. Rev. Lett. **82**, 1632 (1999)
21. H.N. Brown et al. [Muon (g-2) Collab.], Phys. Rev. D **62**, 091101 (2000)
22. H.N. Brown et al. [Muon (g-2) Collab.], Phys. Rev. Lett. **86**, 2227 (2001)
23. G.W. Bennett et al. [Muon g-2 Collab.], Phys. Rev. Lett. **89**, 101804 (2002) [Erratum-ibid. **89**, 129903 (2002)]
24. G.W. Bennett et al. [Muon g-2 Collab.], Phys. Rev. Lett. **92**, 161802 (2004)
25. R. Prigl et al., Nucl. Instrum. Methods Phys. Res. A **374**, 118 (1996); X. Fei, V. Hughes, R. Prigl, Nucl. Instrum. Methods Phys. Res. A **394**, 349 (1997)
26. W. Liu et al., Phys. Rev. Lett. **82**, 711 (1999)
27. T. Kinoshita, M. Nio, Phys. Rev. D **53**, 4909 (1996); M. Nio, T. Kinoshita, Phys. Rev. D **55**, 7267 (1997); T. Kinoshita, arXiv:hep-ph/9808351
28. A. Czarnecki, S.I. Eidelman, S.G. Karshenboim, Phys. Rev. D **65**, 053004 (2002); S.G. Karshenboim, V.A. Shelyuto, Phys. Lett. B **517**, 32 (2001)
29. H. Lamm, Phys. Rev. A **95**(1), 012505 (2017)
30. P.J. Mohr, B.N. Taylor, Rev. Mod. Phys. **72**, 351 (2000); **77**, 1 (2005); P.J. Mohr, B.N. Taylor, D.B. Newell, Rev. Mod. Phys. **84**, 1527 (2012)
31. L.H. Thomas, Phil. Mag. **3**, 1 (1927); V. Bargmann, L. Michel, V.A. Telegdi, Phys. Rev. Lett. **2**, 435 (1959); B.W. Montague, Phys. Rep. **113**, 1 (1984); J.S. Bell, CERN-75-11, 38p (1975)
32. C. Duval, Nucl. Phys. B **912**, 450 (2016)
33. F.J.N. Farley, Phys. Lett. B **42**, 66 (1972)
34. F. Scheck, *Leptons, Hadrons and Nuclei* (North Holland, Amsterdam, 1983)
35. G. Charpak et al., Phys. Rev. Lett. **6**, 128 (1961); G. Charpak et al., Nuovo Cim. **22**, 1043 (1961)
36. J. Bailey et al., Phys. Lett. B **28**, 287 (1968); Nuovo Cim. A **9**, 369 (1972)

37. S. Eidelman et al. [Particle Data Group], Phys. Lett. B **592**, 1 (2004); K.A. Olive et al., Chin. Phys. C **38**, 090001 (2014); C. Patrignani et al., Chin. Phys. C **40**(10), 100001 (2016)
38. H. Grotch, R.A. Hegstrom, Phys. Rev. A **4**, 59 (1971); R. Faustov. Phys. Lett. B **33**, 422 (1970)
39. K. Pachucki, Phys. Rev. A **54**, 1994 (1996); ibid. **56**, 297 (1997); S.G. Karshenboim, Z. Phys. D **36**, 11 (1996); S.A. Blundell, K.T. Cheng, J. Sapirstein, Phys. Rev. Lett. **78**, 4914 (1997); M.I. Eides, H. Grotch, V.A. Shelyuto, Phys. Rev. D **58**, 013008 (1998)
40. K. Melnikov, A. Yelkhovsky, Phys. Rev. Lett. **86**, 1498 (2001)
41. R.J. Hill, Phys. Rev. Lett. **86**, 3280 (2001)
42. K.P. Jungmann, Nucl. Phys. News **12**, 23 (2002)
43. F.G. Major, V.N. Gheorghe, G. Werth, *Charged Particle Traps* (Springer, Berlin, 2005)
44. R.S. Van Dyck, P.B. Schwinberg, H.G. Dehmelt, Phys. Rev. D **34**, 722 (1986)
45. S. Peil, G. Gabrielse, Phys. Rev. Lett. **83**, 1287 (1999)
46. L.S. Brown, G. Gabrielse, Rev. Mod. Phys. **58**, 233 (1986)
47. T. Beier et al., Phys. Rev. Lett. **88**, 011603 (2002); Nucl. Instrum. Methods B **205**, 15 (2003)
48. D. Hanneke, S. Fogwell, G. Gabrielse, Phys. Rev. Lett. **100**, 120801 (2008). doi:10.1103/PhysRevLett.100.120801, http://g2pc1.bu.edu/lept06/GabrielseTalk.pdf
49. D. Hanneke, S.F. Hoogerheide, G. Gabrielse, Phys. Rev. A **83**, 052122 (2011). doi:10.1103/PhysRevA.83.052122